Astronomy & Astrophysics manuscript no. Breuval2019
March 14, 2022

The Leavitt law of Milky Way Cepheids from Gaia DR2 static companion parallaxes

Louise Breuval[1], Pierre Kervella[1], Frédéric Arenou[2], Giuseppe Bono[3,4], Alexandre Gallenne[5,6], Boris Trahin[1], Antoine Mérand[7], Jesper Storm[8], Laura Inno[9], Grzegorz Pietrzyński[10,11], Wolfgang Gieren[10,12], Nicolas Nardetto[6], Dariusz Graczyk[10,11,12], Simon Borgniet[1], Behnam Javanmardi[1], Vincent Hocdé[6]

[1] LESIA (UMR 8109), Observatoire de Paris, PSL Research University, CNRS, UPMC, Univ. Paris-Diderot, 5 place Jules Janssen, 92195 Meudon, France, e-mail: louise.breuval@obspm.fr
[2] GEPI, Observatoire de Paris, Université PSL, CNRS, 5 Place Jules Janssen, 92190 Meudon, France
[3] Department of Physics, Università di Roma Tor Vergata, via della Ricerca Scientifica 1, I-00133 Roma, Italy
[4] INAF-Osservatorio Astronomico di Roma, via Frascati 33, I-00040 Monte Porzio Catone, Italy
[5] European Southern Observatory, 3107 Alonso de Cordóva, Casilla 19001, Santiago, Chile
[6] Université Côte d'Azur, Observatoire de la Côte d'Azur, CNRS, Laboratoire Lagrange, France
[7] European Southern Observatory, Karl-Schwarzschild-Str. 2, 85748 Garching, Germany
[8] Leibniz-Institut für Astrophysik Potsdam (AIP), An der Sternwarte 16, 14482 Potsdam, Germany
[9] Dipartimento di Scienze e Tecnologie, Parthenope University of Naples, Via Giovanni Porzio, 4, 80143 Napoli NA, Italy
[10] Universidad de Concepción, Departamento de Astronomía, Casilla 160-C, Concepción, Chile
[11] Centrum Astronomiczne im. Mikolaja Kopernika (CAMK), PAN, Bartycka 18, 00-716 Warsaw, Poland
[12] Millenium Institute of Astrophysics, Av. Vicuna Mackenna 4860, Santiago, Chile

Received ... ; accepted ...

ABSTRACT

Context. Classical Cepheids (CCs) are at the heart of the empirical extragalactic distance ladder. Milky Way CCs are the only stars of this class accessible to trigonometric parallax measurements. Until recently, the most accurate trigonometric parallaxes of Milky Way CCs were the HST/FGS measurements collected by Benedict et al. (2002, 2007). Unfortunately, the second Gaia data release (GDR2) has not yet delivered reliable parallaxes for Galactic CCs, failing to replace the HST/FGS sample as the foundation of all Galactic calibrations of the Leavitt law (the Period-Luminosity relation).
Aims. We aim at calibrating independently the Leavitt law of Milky Way CCs based on the GDR2 catalog of trigonometric parallaxes.
Methods. As a proxy for the parallaxes of a sample of 23 Galactic CCs, we adopt the GDR2 parallaxes of their spatially resolved companions. As the latter are unsaturated, photometrically stable stars, this novel approach allows us to bypass the GDR2 bias on the parallax of the CCs that is induced by saturation and variability.
Results. We present new Galactic calibrations of the Leavitt law in the J, H, K_S, V, Wesenheit W_H and Wesenheit W_{VK} bands based on the GDR2 parallaxes of the CC companions. A similar calibration using the GDR2 parallaxes of the CCs themselves results in a significantly larger scatter. We show that the adopted value of the zero point of the GDR2 parallaxes, within a reasonable range, has a limited impact on our Leavitt law calibration. However, we find a significant difference with respect to the calibration based on the HST/FGS parallaxes, that corresponds to an FGS parallax zero point offset of $\Delta \approx +200\,\mu$as.
Conclusions. The discrepancy that we observe between the GDR2 and HST/FGS parallaxes has important consequences on the existing Galactic calibrations of the Leavitt law. We note that our results translate into a Hubble constant of 68.43 ± 2.08 km s^{-1} Mpc^{-1} and 69.30 ± 2.08 km s^{-1} Mpc^{-1} for a GDR2 parallax offset of 0.029 mas and 0.046 mas, respectively.

Key words. Stars: variables: Cepheids, Astrometry, Distance Scale, Period-Luminosity Relation.

1. Introduction

Classical Cepheids have historically a major importance among variable stars because of the simple correlation between their pulsation periods, which are easily measured observationally, and their intrinsic luminosity. The discovery of the Leavitt law, also called the period-luminosity (hereafter PL) relation by Leavitt (1908) (see also Leavitt & Pickering 1912) was the cornerstone of the discovery of the expansion of the universe by Hubble and Lemaitre. However, after more than a century of active research, the absolute calibration of the Leavitt law is still unsatisfactory. The main cause of this situation is the rarity of CCs in the Galaxy, and consequently their large distances from the Sun. This makes the measurement of their trigonometric parallaxes particularly difficult, and even the Hipparcos satellite (Feast & Catchpole 1997; Pont 1999; Groenewegen & Oudmaijer 2000; Di Benedetto 2002; van Leeuwen et al. 2007) was unable to determine sufficiently accurate parallaxes of CCs. Focused efforts, e.g., by Benedict et al. (2002, 2007), Riess et al. (2014) and Casertano et al. (2016), resulted in the measurement of the parallaxes of a limited sample of CCs, with individual precisions in the order of 5 to 15%. As a result, the absolute calibration of the Leavitt law from geometrical distances is uncertain at a $\approx$ 5% level. It is therefore one of the main contributors to the uncertainty on the Hubble constant H_0 (Riess et al. 2016). A careful calibration of this relation and especially of its zero-point is fundamental, as it is used to anchor extragalactic distances and to derive cosmological parameters. Moreover, the current tension

between the determinations of H_0 from the Cosmic Microwave Background (CMB) modeling and the empirical distance ladder (see, e.g., Riess et al. 2019; Lemos et al. 2019) may have important implications on, for instance, the equation of state of dark energy.

The calibration of the zero-point of the Leavitt law requires the independent and accurate measurement of the distances of a sample of CCs. Unfortunately, most of Gaia's second data release (GDR2; Gaia Collaboration et al. 2018) parallaxes of CCs are still affected by systematics. As a consequence, calibrating the PL relation using directly the GDR2 parallaxes of Cepheids leads to ambiguous results (Groenewegen 2018; Riess et al. 2018b; Gaia Collaboration et al. 2017; Clementini et al. 2019).

Kervella et al. (2019b) recently presented a sample of 28 Galactic CCs that are members of spatially resolved stellar systems. These companions are photometrically stable stars (or only variable at a low level), and their GDR2 parallaxes are therefore not affected by such a strong chromatic PSF effect in the GDR2 as CCs. As the CC and its companion share the same parallax (their relative distance is negligible compared to the distance to the Sun), the GDR2 parallaxes of the CC companions provide a natural proxy for those of the CCs themselves.

Until the begining of the Gaia era, most (if not all) PL relations for Galactic Cepheids relied on HST measurements (Benedict et al. 2007, 2002; Fouqué et al. 2007). Moreover, the Baade-Wesselink methods are calibrated using the projection factor (*p*-factor) from Cepheids with HST parallaxes (Breitfelder et al. 2016). As a consequence, the corresponding values of H_0 derived from these PL relations were also related to the HST (Freedman et al. 2001; Sandage et al. 2006; Riess et al. 2016, 2018a). Our approach is therefore the first solid alternative to Cepheid parallaxes based on HST measurements.

In this paper, we derive calibrations of the Leavitt law in the J, H, K_S, V, Wesenheit W_{VK} and Wesenheit W_H bands based on this sample of companion parallaxes. We also consider two additional stars with non-GDR2 parallaxes, V1334 Cyg and RS Pup. In Sect. 2, we introduce our sample of stars and their associated data. In Sect. 3, we determine the absolute magnitudes of the CCs from their parallaxes and averaged apparent luminosities in order to establish the PL relations. Then, we discuss the accuracy of the companion parallaxes from the GDR2 compared to CC parallaxes and we analyze the influence of the zero-point of the GDR2 parallaxes. In Sect. 4, we compare our PL relations with those obtained with HST/FGS parallaxes (Benedict et al. 2007) and other previous works. Finally, we discuss the effect of using our Leavitt law calibration as an anchor for the Hubble constant H_0.

2. Cepheid sample and observational data

The data described in this section are listed with their uncertainties and references in Tab. 1 and 2.

2.1. Parallaxes

In the determination of Gaia DR2 parallaxes, the astrometric solution depends on magnitude and color-dependent terms. The parallaxes are determined assuming a constant mean color for each star (Lindegren et al. 2018; Gaia Collaboration et al. 2019). However, variable stars, and in particular Cepheids, RR Lyrae and Miras, show large color variations during a cycle, so this assumption is incorrect (Mowlavi et al. 2018). To derive unbiased parallaxes, chromaticity corrections must be applied to every single measurement, but this approach was not adopted in the GDR2 data reduction (see the ESA DR2 web page[1]). Moreover, as CCs are intrinsically very bright and distant supergiants, their flux is high, even saturated for all nearby CCs, while their parallax is small. This combination results in an amplification of the relative bias on their parallax due to their variability, and it is likely the cause of the particular behavior of this class of stars in the GDR2.

The Gaia DR2 astrometry is generally of poor quality for very bright stars ($G < 6$ mag), due to calibration issues and saturation (Drimmel et al. 2019; Lindegren 2019; Riess et al. 2018b). This problem occurs independently of the chromaticity issue raised previously, whether the star is variable or not. Although only one of our Cepheids is brighter than 6 mag in the G band (AX Cir), several of them are either very close to this limit (ER Car, V0659 Cen, RS Pup, U Sgr), with a G magnitude brighter than 7 or reaching this limiting magnitude along the pulsation cycle. On the other hand, companions are in average 7 mag fainter than their Cepheids, with mean magnitudes between 8 and 15 mag in the G band (except for Delta Cep companion with $G = 6.31$ mag). The companions are therefore not as affected as CCs by the saturation issue and they are far off from the sensitivity limit. They consequently belong to the best dynamical range for Gaia DR2 capability, which shows again that they are a reliable proxy for the CCs parallaxes.

Although the presence of the companion may in principle affect the proper motion of the two components of the system, their parallax would only be affected if the period of the system was close to one year, which is the timeline of Gaia DR2. However, given the separation between the CCs and their companions, the periods of the systems considered in our study are on the order of 10 ka, which means that the parallaxes of the CCs and of the companions are not sensitive to the binarity of the system.

We use the 28 resolved companions of CCs from Kervella et al. (2019b). These authors distinguished gravitationally bound candidate companions from unrelated field stars by using a progressive selection algorithm based on their parallax and relative velocity. After a selection (Sect. 2.2, 2.5), we use the GDR2 parallaxes of 23 of the companions listed in Kervella et al. (2019b), and we assume that their parallax is identical to that of their parent star. This assumption is justified by the fact that their projected linear separation from the CCs represent typically 0.01% of their distance to the Sun. This sample covers a broad range of periods from 2 to 41 days. The mean relative uncertainty on the Cepheids parallaxes is 9%, but because of their variability, systematic biases are likely to be present on a larger scale. For the companions, the mean relative uncertainty on the parallaxes is 12%. The companions are not variable stars (except CE Cas B, whose companion CE Cas A is also a CC), so their GDR2 parallaxes are expected to be more reliable than those of the CCs. For a given parallax $\varpi_{\rm Gaia}$ given by GDR2, we use corrected parallaxes $\varpi = \varpi_{\rm Gaia} - {\rm ZP}_{\rm Gaia}$, where ${\rm ZP}_{\rm Gaia}$ is the zero-point of Gaia parallaxes, a value which must be subtracted from all GDR2 parallaxes. We can also define the offset $\Delta_{\rm Gaia}$ applied on parallaxes as: $\Delta_{\rm Gaia} = -\,{\rm ZP}_{\rm Gaia}$. The parallaxes given in Tab. 1 are GDR2 parallaxes corrected from an offset $\Delta_{\rm Gaia} = +0.029$ mas, derived by Lindegren et al. (2018). For a given Cepheid, when more than one companion was found by Kervella et al. (2019b), as CV Mon and SY Nor, we selected the companion with the smallest uncertainty on its parallax.

[1] https://www.cosmos.esa.int/web/gaia/dr2

Table 1. Gaia DR2 parallaxes and RUWE ϱ (quality indicator) of the Cepheids and their companions from the sample of Kervella et al. (2019b). Here the parallaxes are already corrected for ZP_{Gaia} = -0.029 mas.

Cepheid	P (days)	ϖ_{GDR2} (mas)	ϱ	G (mag)	Companion (GDR2)	ϖ_{GDR2} (mas)	ϱ	G (mag)
TV CMa	4.670	$0.343_{\pm 0.034}$	0.89	$10.085_{\pm 0.0002}$	3044483895574944512	$0.455_{\pm 0.050}$	1.08	$15.771_{\pm 0.0029}$
ER Car	7.719	$0.825_{\pm 0.035}$	0.85	$6.606_{\pm 0.0002}$	5339394048386734336	$0.918_{\pm 0.152}$	1.08	$18.444_{\pm 0.0023}$
DF Cas	3.832	$0.336_{\pm 0.028}$	0.88	$10.434_{\pm 0.0001}$	465719182408531072	$0.396_{\pm 0.080}$	1.15	$17.259_{\pm 0.0009}$
V0659 Cen	5.622	$0.513_{\pm 0.154}$	4.12 *	$6.391_{\pm 0.0003}$	5868451109212716928	$1.384_{\pm 0.318}$	1.04	$19.695_{\pm 0.0036}$
δ Cep	5.366	-	20.9 *	-	2200153214212849024	$3.393_{\pm 0.049}$	1.29	$6.282_{\pm 0.0005}$
AX Cir	5.273	$1.774_{\pm 0.345}$	8.01 *	$5.626_{\pm 0.0006}$	5874031027625742848	$1.754_{\pm 0.374}$	1.13	$19.824_{\pm 0.0037}$
BP Cir	2.398	$1.024_{\pm 0.040}$	1.05	$7.288_{\pm 0.0001}$	5877472464676660480	$1.525_{\pm 0.188}$	1.06	$18.918_{\pm 0.0022}$
R Cru	5.826	-	4.57 *	-	6054935874780531328	$1.107_{\pm 0.089}$	2.81 *	$15.691_{\pm 0.0044}$
X Cru	6.220	$0.552_{\pm 0.046}$	0.86	$8.068_{\pm 0.0001}$	6059762524642419968	$0.638_{\pm 0.053}$	1.13	$16.045_{\pm 0.0006}$
VW Cru	5.265	$0.812_{\pm 0.045}$	0.93	$9.014_{\pm 0.0003}$	6053622508133367680	$0.708_{\pm 0.040}$	0.89	$14.074_{\pm 0.0002}$
V0532 Cyg	4.677 ⋆	$0.590_{\pm 0.032}$	0.75	$8.673_{\pm 0.0003}$	1971721839529622272	$0.648_{\pm 0.040}$	0.89	$14.674_{\pm 0.0004}$
V1046 Cyg	4.845	$0.296_{\pm 0.029}$	1.13	$11.570_{\pm 0.0001}$	2060460708575795712	$0.356_{\pm 0.060}$	1.51 *	$15.778_{\pm 0.0047}$
CV Mon	5.379	$0.511_{\pm 0.041}$	1.09	$9.605_{\pm 0.0113}$	3127142327895572352	$0.537_{\pm 0.040}$	0.96	$13.489_{\pm 0.0003}$
RS Nor	6.198	$0.450_{\pm 0.046}$	0.92	$9.485_{\pm 0.0005}$	5932812740361508736	$0.478_{\pm 0.044}$	1.03	$14.547_{\pm 0.0003}$
SY Nor	12.65	$0.429_{\pm 0.035}$	1.04	$8.965_{\pm 0.0006}$	5884729035245399424	$0.443_{\pm 0.053}$	1.26	$12.105_{\pm 0.0019}$
QZ Nor	5.406 ⋆	$0.503_{\pm 0.038}$	0.91	$8.577_{\pm 0.0001}$	5932565899990412672	$0.481_{\pm 0.098}$	1.01	$17.935_{\pm 0.0013}$
AW Per	6.464	$1.071_{\pm 0.064}$	1.02	$7.048_{\pm 0.0011}$	174489098011144960	$1.075_{\pm 0.249}$	1.07	$17.417_{\pm 0.0030}$
RS Pup	41.44	$0.613_{\pm 0.026}$	0.90	$6.459_{\pm 0.0003}$	5546476755539995008	$0.532_{\pm 0.048}$	0.99	$16.248_{\pm 0.0006}$
U Sgr	6.745	$1.489_{\pm 0.045}$	0.90	$6.354_{\pm 0.0005}$	4092905203841177856	$1.490_{\pm 0.038}$	0.92	$11.141_{\pm 0.0006}$
V0350 Sgr	5.154	$1.015_{\pm 0.047}$	0.79	$7.251_{\pm 0.0002}$	4080121319521641344	$1.044_{\pm 0.048}$	1.09	$12.268_{\pm 0.0002}$
V0950 Sco	4.817 ⋆	$0.869_{\pm 0.052}$	0.99	$7.052_{\pm 0.0007}$	5960623340819000192	$0.922_{\pm 0.058}$	0.98	$15.279_{\pm 0.0024}$
CM Sct	3.917	$0.405_{\pm 0.065}$	1.00	$10.510_{\pm 0.0005}$	4253603428053877504	$0.547_{\pm 0.050}$	0.93	$14.728_{\pm 0.0005}$
EV Sct	4.398 ⋆	$0.526_{\pm 0.054}$	0.95	$9.622_{\pm 0.0002}$	4156513016572003840	$0.510_{\pm 0.043}$	1.01	$13.615_{\pm 0.0015}$
α UMi	5.672 ⋆	-	57.1 *	-	576402619921510144	$7.321_{\pm 0.028}$	1.21	$8.619_{\pm 0.0004}$
SX Vel	9.550	$0.438_{\pm 0.041}$	0.89	$7.973_{\pm 0.0003}$	5329838158460399488	$0.461_{\pm 0.068}$	0.93	$17.019_{\pm 0.0014}$
CS Vel	5.905	$0.194_{\pm 0.030}$	1.04	$11.103_{\pm 0.0002}$	5308893046071732096	$0.251_{\pm 0.048}$	0.92	$16.203_{\pm 0.0007}$
DK Vel	2.482	$0.238_{\pm 0.025}$	0.94	$10.408_{\pm 0.0001}$	5311599390863537408	$0.402_{\pm 0.089}$	0.99	$18.087_{\pm 0.0014}$

Notes. ⋆ Modified period for first overtones; * RUWE $\varrho > 1.4$.

We also included two additional stars with independently determined parallaxes. The first one is the long-period Cepheid RS Puppis, whose distance of 1910 ± 80 pc (ϖ = 0.524 ± 0.022 mas) was determined by Kervella et al. (2014) using polarimetric HST images of the light echoes propagating in its circumstellar nebula (see also Kervella et al. 2017). We refer to this particular parallax determination as RS Pup_{echo} in the following. The second additional star is the binary Cepheid V1334 Cyg, for which Gallenne et al. (2018) obtained a distance of 720.4±7.8 pc (ϖ = 1.388 ± 0.015 mas) through the observation of its orbit by spectroscopy and optical interferometry. With an uncertainty of 1%, this is to date the most accurate distance measurement of a Cepheid.

2.2. Quality indicators

To get a better precision on PL relations, we recall that we use the GDR2 parallaxes of the companions given in Kervella et al. (2019b) instead of those of the Cepheids, assuming that they are at the same distance. Since they are not variable stars, the companions are supposed to have more precise parallaxes than their Cepheid. Various quality indicators are introduced in the second release of Gaia data, such as the astrometric excess noise or the goodness-of-fit (GOF). Another interesting quality indicator is the re-normalised unit weight error (RUWE, noted ϱ in the following; see also Kervella et al. 2019a). It is particularly pertinent to use because it evaluates the quality of the parallax of a star compared to other stars of the same type. This parameter is defined as follows (Lindegren 2018b):

$$\varrho = \frac{\mathrm{UWE}}{u_0(G, C)}$$

where $\mathrm{UWE} = \sqrt{\chi^2/(N-5)}$ is the unit weight error and u_0 is an empirical normalisation factor which is not directly available in the Gaia release but which can be computed from the lookup table on the ESA DR2 *Known issues* web page[2]. Following Lindegren (2018b), we estimate that a parallax is reliable if $\varrho < 1.4$. The Table 1 gives the RUWE of the stars of Kervella et al. (2019b) and of their companions. We can suggest that the RUWE parameter can be an indicator of a close-in companion of a Cepheid. An example is the star AX Cir, for which a close-in (30 mas) component has been detected by Gallenne et al. (2014).

We note that δ Cep, R Cru and α UMi (Polaris) have no valid parallax value in the GDR2 catalog. Five CCs have $\varrho > 1.4$, but for all of them, the RUWE of their companion is lower, so we can use its parallax. Among the companions, all of them have a GDR2 parallax and only two have a RUWE over the limit: R Cru and V1046 Cyg, with ϱ = 2.80 and 1.51 respectively. We exclude them from the sample in order to keep accurate parallaxes only. The star CE Cas B is a particular case because its companion, CE Cas A, is also a Cepheid. The two components of CE Cas are present in the GDR2, but with statistically different parallaxes (ϖ_A = 0.317 ± 0.031 mas; ϖ_B = 0.262 ± 0.030 mas). The GDR2 parallax of component B is likely biased, possibly due to light

[2] https://www.cosmos.esa.int/web/gaia/dr2-known-issues

Table 2. Averaged apparent magnitudes in V, I, J, H, K_S bands, in Wesenheit W_{VK} and W_H bands, and color excess E(B-V) for the Cepheids from Kervella et al. (2019b) and V1334 Cyg (Gallenne et al. 2018).

Star	E(B-V)	$< V >$	$< I >$	ref	$< J >$	$< H >$	$< K_S >$	e_{JHK_s}	ref
TV CMa	$0.611_{\pm 0.031}$	10.59	9.180	a	8.022	7.582	7.364	0.008	e
ER Car	$0.118_{\pm 0.017}$	6.82	5.932	a	5.310	5.034	4.896	0.008	f
DF Cas	$0.600_{\pm 0.052}$	10.88	9.800	b	8.488	8.036	7.879	0.025	g
V0659 Cen	$0.161_{\pm 0.036}$	6.62	5.735	a	5.177	4.907	4.651	0.025	g
δ Cep	$0.080_{\pm 0.019}$	3.95	3.260	b	2.683	2.396	2.294	0.010	h
AX Cir	$0.282_{\pm 0.129}$	5.88	5.090	b	4.299	3.879	3.780	0.025	g
BP Cir	$0.274_{\pm 0.039}$	7.55	6.639	a	5.870	5.626	5.483	0.008	f
X Cru	$0.313_{\pm 0.020}$	8.40	7.292	a	6.521	6.125	6.001	0.025	i,g
VW Cru	$0.681_{\pm 0.049}$	9.60	7.978	a	6.805	6.261	6.051	0.025	g
V0532 Cyg	$0.552_{\pm 0.007}$	9.09	7.845	a	6.863	6.393	6.250	0.025	j
V1334 Cyg	$0.025_{\pm 0.009}$	5.86	5.310	b	4.817	4.536	4.510	0.020	k
CV Mon	$0.750_{\pm 0.019}$	10.31	8.650	a	7.314	6.781	6.529	0.008	e
RS Nor	$0.614_{\pm 0.038}$	10.00	8.523	a	7.412	6.794	6.683	0.020	k
SY Nor	$0.650_{\pm 0.063}$	9.50	7.904	a	6.574	6.105	5.865	0.008	f
QZ Nor	$0.307_{\pm 0.021}$	8.87	7.865	a	7.085	6.748	6.614	0.008	l
AW Per	$0.510_{\pm 0.017}$	7.48	6.173	a	5.213	4.832	4.657	0.008	e
RS Pup	$0.480_{\pm 0.011}$	7.01	5.479	a	4.365	3.828	3.619	0.008	l
U Sgr	$0.434_{\pm 0.007}$	6.69	5.436	a	4.506	4.100	3.912	0.008	e
V0350 Sgr	$0.328_{\pm 0.009}$	7.47	6.413	a	5.625	5.245	5.121	0.010	i
V0950 Sco	$0.267_{\pm 0.020}$	7.31	6.404	a	5.681	5.439	5.295	0.008	f
CM Sct	$0.824_{\pm 0.048}$	11.1	9.532	c	8.300	7.818	7.558	0.025	g
EV Sct	$0.663_{\pm 0.016}$	10.13	8.668	a	7.608	7.184	7.018	0.008	l
α UMi	$0.017_{\pm 0.010}$	1.98	1.270	b	0.941	0.460	0.652	0.025	m
SX Vel	$0.252_{\pm 0.015}$	8.29	7.261	a	6.500	6.133	5.991	0.008	l
CS Vel	$0.762_{\pm 0.029}$	11.7	10.078	c	8.771	8.246	8.011	0.008	l
DK Vel	$0.301_{\pm 0.020}$	10.69	9.920	b	8.820	8.496	8.386	0.025	g

References. (a) Gaia Collaboration et al. (2017); (b) ESA (1997); (c) Droege et al. (2006); (d) Ngeow & Kanbur (2006); (e) Monson & Pierce (2011); (f) Laney (private communication); (g) Genovali et al. (2014); (h) Barnes et al. (1997); (i) Welch et al. (1984); (j) 2MASS (Skrutskie et al. 2006); (k) SPIPS algorithm (Mérand et al. 2015); (l) Laney & Stobie (1992); (m) Groenewegen (2018)

contamination from the nearby component A. We exclude both stars from our sample as a precaution.

The angular separation between the CCs and their companions is in most cases larger than 10 arcsec, which is large enough to prevent flux contamination, given the brightness of the CCs. If, by any chance, a companion was contamined by the brightness of its Cepheid, this contamination would be seen in its RUWE parameter. As we rejected any star with a RUWE larger than 1.4, the flux contamination should not introduce any bias to our results.

2.3. Photometry

To determine the phase-averaged magnitude of the CCs of our sample, we first searched them in the catalogue of 452 CCs assembled by Groenewegen (2018). It is a compilation of mean apparent magnitudes in J, H, K and V bands in different photometric systems, taken from different sources (see Table 2).

Laney & Stobie (1992), Laney (private communication) and Feast et al. (2008) provide NIR magnitudes in the SAAO system. For homogeneity, we converted them into 2MASS J, H, K_S magnitudes using the equations from Koen et al. (2007). The magnitudes given by Monson & Pierce (2011) are in the BIRCAM photometric system, and the magnitudes taken from Welch et al. (1984) and Barnes et al. (1997) are in the CIT photometric system. They were all converted into the 2MASS system using the equations in Monson & Pierce (2011). For the remaining stars, the mean magnitude is computed as the median of the available data in Welch et al. (1984), Schechter et al. (1992), and the 2MASS (Skrutskie et al. 2006) or DENIS (Epchtein et al. 1999) databases. All magnitudes are intensity-mean magnitudes, except the NIR magnitudes from Genovali et al. (2014) which are based on single-epoch 2MASS data and template fitting.

For the stars RS Nor and V1334 Cyg, the averaged magnitudes in NIR bands were derived by performing a fit of the photometric light curves using the SPIPS algorithm (Mérand et al. 2015). The uncertainty of the mean magnitudes for the data coming from Laney & Stobie (1992), Laney Laney (private communication), Feast et al. (2008) and Monson & Pierce (2011) is 0.008 mag. For the data taken from Genovali et al. (2014), the uncertainty on magnitudes is 0.025 mag and for the values given by Welch et al. (1984) and Barnes et al. (1997), it is of 0.01 mag.

In the V band, all mean magnitudes are provided in the standard Johnson system by Mel'nik et al. (2015). An uncertainty of 0.008 mag on those magnitudes is adopted.

By combining those apparent magnitudes, reddening-free Wesenheit magnitudes can be built. From V and K_S magnitudes, we construct W_{VK}, defined as $m_{W_{VK}} = m_{K_S} - 0.13(m_V - m_{K_S})$ by Ripepi et al. (2012). We also computed W_H Wesenheit magnitude, which is a combination of HST bands, defined as:

$$m_{W_H} = m_{F160W} - R(m_{F555W} - m_{F814W})$$

where $R = 0.386$ according to Fitzpatrick (1999). The correspondance between HST filters $F160W$, $F555W$ and $F814W$ and J, H, V and I bands is given in Sect. 3.1.2. of Riess et al. (2016) and yields:

$$m_{W_H} = 0.16\ J + 0.84\ H - R\ [0.014 + 1.128\ (V - I)]$$

The average apparent magnitudes in J, H and V bands are those from Table 2, and apparent magnitudes in the I band are taken from Gaia Collaboration et al. (2017); ESA (1997); Droege et al. (2006); Ngeow & Kanbur (2006) with an uncertainty set to 0.02 mag.

2.4. Color Excess

In order to determine absolute magnitudes, we need to correct the apparent magnitudes from the interstellar absorption. The values of $E(B-V)$ are taken from the DDO database (Fernie et al. 1995), which is a compilation of various $E(B-V)$ from the literature determined in the same system. For the star V1334 Cyg, the color excess given in the DDO database is negative, so we took it from Kovtyukh et al. (2008).

2.5. Pulsation modes

The identification of first overtone Cepheids is essential for the calibration of the Leavitt law. Here we review the different pulsation modes found in the literature for the stars of our sample.

Gaia DR2 classifies the Cepheids BP Cir, EV Sct, V0532 Cyg, V0950 Sco, QZ Nor and DK Vel as first overtones. Bono et al. (2001) agrees with this classification for EV Sct and QZ Nor.

The star α UMi has no pulsation mode given by GDR2 but Bono et al. (2001), Spreckley & Stevens (2007) and Fouqué et al. (2007) classified it as a first overtone.

V1334 Cyg, which is one of our two additional stars, is classified as a fundamental pulsator according to GDR2 but Gallenne et al. (2018), Luck (2018) and Kovtyukh et al. (2012) conclude that it is a first overtone. We thus consider this star as a first overtone. Its period was converted by Gallenne et al. (2018) from the first overtone into its equivalent fundamental mode.

For the two stars BP Cir and DK Vel, GDR2 found a first overtone pulsation mode. This classification is confirmed by Zabolotskikh et al. (2004) for both Cepheids, and also by Evans et al. (1992) and Usenko et al. (2014) for BP Cir, but the recent paper from Luck (2018) classifies them as fundamentals. Given the disagreement between the sources about the pulsation mode of BP Cir and DK Vel, we decide to exclude them from the sample.

The Cepheid V0659 Cen is pulsating on its fundamental mode according to Gaia, but Zabolotskikh et al. (2004) found that it is a first overtone. As the star is consistent with a fundamental mode in our diagram, as well as in the reclassification of Ripepi et al. (2019), we consider here that V0659 Cen is a fundamental pulsator.

For all the CCs of our sample except V1334 Cyg, the pulsation modes given by Gaia DR2 are confirmed by the recent reclassification of Ripepi et al. (2019). The pulsation modes of the stars of our CC sample taken from different sources are given in Table 3. The second column of this table (GDR2) shows the pulsation mode provided by the GDR2 catalog, the third column gives it according to the literature, and the last column gives the pulsation mode that we adopted.

In order to establish accurate PL and PW relations without excluding the first overtones, we converted their observed periods $P_{\rm FO}$ into the fundamental mode equivalent period $P_{\rm F}$ using the equation by Feast & Catchpole (1997):

$$P_{\rm FO}/P_{\rm F} = 0.716 - 0.027 \log P_{\rm FO}$$

The period modification of these six first overtone CCs is listed in Table 4 and shown in Fig. 1 using horizontal grey dashed lines. The result obtained after the period transformation is consistent with the distribution of the fundamental pulsators in the PL plane.

Table 3. Pulsation mode of the Cepheids of our sample.

Cepheid	GDR2	Literature	Adopted
TV CMa	F	-	F
ER Car	F	-	F
DF Cas	F	-	F
V0659 Cen	F	FO [a], F [j]	F
δ Cep	-	-	F
AX Cir	F	-	F
BP Cir	FO	FO [a,b,c,j], F [d]	⋆
X Cru	F	-	F
VW Cru	F	-	F
V0532 Cyg	FO	FO [j]	FO
V1334 Cyg	F	FO [d,e,f,j]	FO
CV Mon	-	-	F
RS Nor	-	-	F
SY Nor	F	-	F
QZ Nor	FO	FO [g,j]	FO
AW Per	F	-	F
RS Pup	F	-	F
U Sgr	F	-	F
V0350 Sgr	-	-	F
V0950 Sco	FO	FO [j]	FO
CM Sct	F	-	F
EV Sct	FO	FO [g,j]	FO
α UMi	-	FO [g,h,i]	FO
SX Vel	F	-	F
CS Vel	F	-	F
DK Vel	FO	FO [a,j], F [d]	⋆

Notes. 'F' = Fundamental; 'FO' = First Overtone; ⋆ = excluded because of uncertain pulsation mode.

References. (a) Zabolotskikh et al. (2004); (b) Evans et al. (1992); (c) Usenko et al. (2014); (d) Luck (2018); (e) Gallenne et al. (2018); (f) Kovtyukh et al. (2012); (g) Bono et al. (2001); (h) Spreckley & Stevens (2007); (i) Fouqué et al. (2007); (j) Ripepi et al. (2019).

Table 4. Transformation of first overtones into fundamental pulsators.

Cepheid	$P_{\rm FO}$ (days)	$P_{\rm F}$ (days)
EV Sct	3.0910	4.3983
V0532 Cyg	3.2836	4.6771
V1334 Cyg	3.3330	4.7900
V0950 Sco	3.3804	4.8174
QZ Nor	3.7860	5.4056
α UMi	3.9696	5.6722

3. Calibration of the Leavitt law of MW Cepheids

3.1. Astrometry Based Luminosities

In order to calibrate near-infrared (NIR) and optical PL relations, as well as Period-Wesenheit (PW) relations, we used the approach introduced by Feast & Catchpole (1997) and Arenou & Luri (1999), and we computed the Astrometric Based Luminosity (ABL), defined as :

$$ABL = 10^{0.2M} = \varpi 10^{0.2m-2}$$

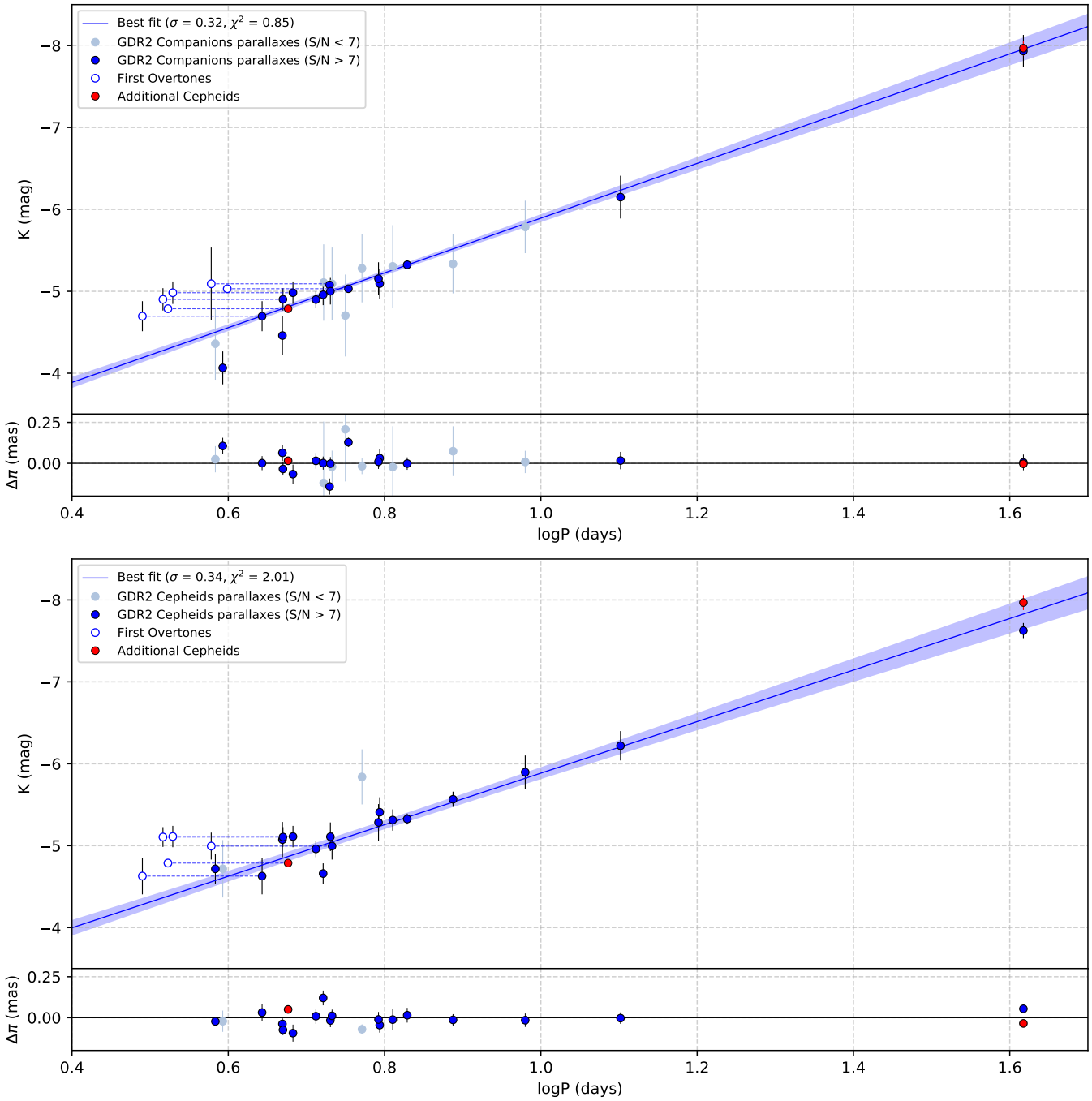

Fig. 1. Period-luminosity diagrams in the K_S band, using the GDR2 parallaxes of the companions (top) and those of the Cepheids (bottom).

where M is the absolute magnitude, m is the dereddened apparent magnitude and ϖ is the parallax in milliarcseconds.

Calibrating the Leavitt Law following this approach is equivalent to determine the coefficients a and b in the equation:

$$ABL = 10^{0.2[a(logP - logP_0)+b]}$$

One advantage of using ABL instead of absolute magnitudes is that the results are not subject to the Lutz-Kelker bias (Lutz & Kelker 1973) as modified by Hanson (1979) (hereafter LKH bias). Moreover, the ABL have symmetrical error bars.

The LKH correction only occurs when a truncation is performed on the observed parallaxes. In the search of companions by Kervella et al. (2019b), no selection was carried on GDR2 parallaxes of CCs, and they range in a particularly large interval ([0.2 - 7.3] mas), which justifies why the LKH correction is unneccessary for this sample. We still note the presence of a natural bias which is beyond our control: the more distant is a Cepheid, the hardest it is to detect a companion around it. However, if Cepheids with small parallaxes were available and hosted companions, their parallaxes would be too small to be reliable for our study.

The extinction $A_\lambda = R_\lambda\, E(B-V)$ is computed using the multiplicative total-to-selective absorption ratios from Fouqué et al. (2007), that is based on the Laney & Caldwell (2007) system: $R_V = 3.23$ (Sandage et al. 2004), $R_J = 0.94$, $R_H = 0.58$, and $R_K = 0.38$. The uncertainties on the absolute magnitudes are dominated by the uncertainties of the parallaxes.

According to, e.g., Benedict et al. (2007) and Riess et al. (2018b), a small correction on the derived absolute magnitudes should be made for the Lutz-Kelker bias (Lutz & Kelker 1973) as modified by Hanson (1979, hereafter LKH bias). This bias depends on the sample of stars and on the parallaxes distribution (Oudmaijer et al. 1998). Koen & Laney (1998) showed that the LKH bias can only arise when the sample of stars is selected on the basis of parallax. For our sample, the stars are not selected according to their parallax, so following the criterion of Koen & Laney (1998), we therefore do not apply any LKH correction on our absolute magnitudes.

3.2. Fit of the PL relation

We performed a weighted fitting of the ABL function by using the `curve_fit` function from the python Scipy library to fit the PL relation in the different bands. The robustness of the fit and of the uncertainties is ensured by a bootstrapping method, applied with 50000 iterations. The distributions of the slope and zero-point of our K_S Leavitt law inferred from companion GDR2 parallaxes and obtained by this technique are represented on Fig. A.1 in Appendix.

The PL diagrams represented in Fig. 1 were obtained with the Gaia DR2 parallaxes of the companions (top panel) and of the CCs themselves (bottom panel). We chose to represent the PL diagram in the K_S band because it exhibits a low intrinsic dispersion. The stars that contribute the most to the linear fit, for which $S/N > 7$, are represented in dark blue, while the other stars are shown in grey. In the lower panel of each diagram are shown the residuals in terms of parallax, computed as the difference between the input GDR2 parallax and the parallax given by the best fit. The empty circles represent first overtone pulsators and the two red points are the two additional stars with independent distance measurement, V1334 Cyg and RS Pup$_{echo}$.

We used the formalism detailed in Gallenne et al. (2017), i.e. we adopted the following linear parametrization:

$$M_\lambda = b_\lambda + a_\lambda \, (\log P - \log P_0)$$

where a_λ and b_λ are respectively the slope and the zero-point of the PL relation. Such a parametrization removes the correlation between a_λ and b_λ and minimizes their respective uncertainties. The optimum value of $\log P_0$ depends on the dataset (see Gallenne et al. 2017 for further details):

$$\log P_0 = \frac{\left\langle \log P_i / e_i^2 \right\rangle}{\left\langle 1/e_i^2 \right\rangle}$$

where $\log P_i$ are the periods of the stars, and e_i are the uncertainties on their mean magnitude measurements; $\langle\rangle$ denotes the averaging operator. We find our sample centered around $\log P_0$ = 0.77. We use this value in the following, except in Sect. 4.2 where we set $\log P_0 = 1$ in order to compare our results with other PL from the literature more easily.

Even if converting first overtones into fundamentals may introduce a small uncertainty on the period, we decide not to exclude them from our sample. Fundamentalizing those six stars instead of rejecting them induces only a very small change on the intercept of the PL relation and allows to improve the precision of the fit.

For example, if we fundamentalize the overtones, the sample includes 25 Cepheids and we obtain $K_S = -5.125_{\pm 0.031} - 3.341_{\pm 0.161}(\log P - 0.77)$, which gives $K_S = -4.223 \pm 0.053$ mag at $\log P = 0.5$ and $K_S = -5.893 \pm 0.048$ mag at $\log P = 1$.

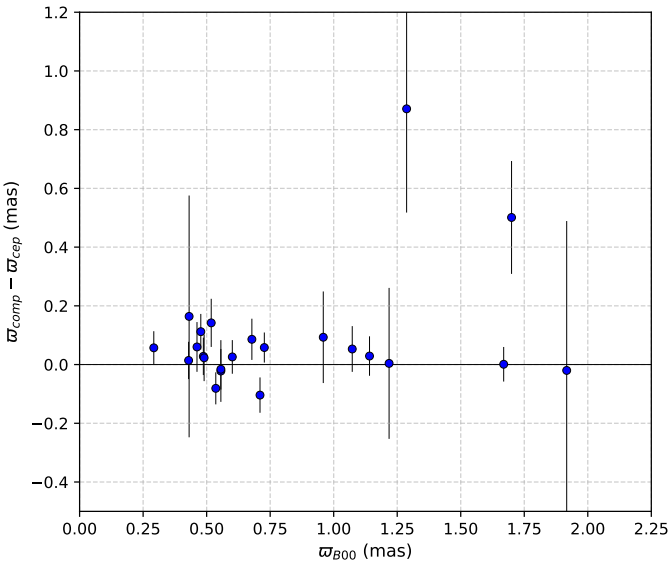

Fig. 2. Comparison of GDR2 parallaxes of CCs and of their companions.

If we excluded those six Cepheids, the sample would be reduced to 19 stars and we would get $K_S = -5.139_{\pm 0.060} - 3.346_{\pm 0.261}(\log P - 0.77)$, which gives $K_S = -4.236 \pm 0.092$ mag and $K_S = -5.909 \pm 0.085$ mag respectively for $\log P = 0.5$ and $\log P = 1$. The current findings agree, within the errors, either neglecting or including first overtones. However, the precision of the fit is significantly better when the first overtones are fundamentalized. In the following, the observed period of first overtone CCs is not represented anymore, but only the fundamentalized period.

3.3. The Leavitt law from Cepheid and companion parallaxes

In this section, we assess the GDR2 parallaxes of the resolved companions compared to the parallaxes of their Cepheid parent stars. Figure 2 shows the difference between GDR2 parallaxes of CCs and of their associated companion, against the parallaxes predicted by Berdnikov et al. (2000). We notice that in some cases the parallaxes of CCs and of their companions show significant differences with the predicted values. As a general trend, the CC parallaxes appear slightly smaller than the companion parallaxes.

Figure 1 shows a comparison of the PL relations obtained in the K_S band using the GDR2 parallaxes of : 1) the companions (left panel), and 2) the CCs (right panel). When we adopt the CC parallaxes, the error bars are smaller than when we use the companion parallaxes, because CCs are brighter than their companions. But as we mentioned in Sect. 2.1, the variability of CCs is problematic for the present astrometric processing, resulting in a possible bias. As a result, the CC parallax values in the GDR2 catalog are unreliable and the formal associated uncertainties are underestimated. We note that the χ^2_r is smaller when we use the companion parallaxes: we obtain a reduced $\chi^2_r = 0.85$ with companion parallaxes compared to $\chi^2_r = 2.01$ with the CCs parallaxes. This is also the case in the V, J and W_{VK} bands (see Table B.1 in Appendix).

We can infer from this comparison that the idea of using the parallaxes of the companions is reliable and that the PL relations derived are more precise when the companion parallaxes are used instead of the CC parallaxes. Moreover, the two closest

Table 5. Zero-point offset for GDR2 parallaxes found in the literature.

ZP_{Gaia} (mas)	Reference	Type of sources
−0.029	Lindegren et al. (2018)	Quasars
$-0.031_{\pm 0.011}$	Graczyk et al. (2019)	Eclipsing binaries
$-0.0319_{\pm 0.0008}$	Arenou et al. (2018)	MW Cepheids
$-0.035_{\pm 0.016}$	Sahlholdt & Silva Aguirre (2018)	Dwarf stars
$-0.041_{\pm 0.010}$	Hall et al. (2019)	Red giants
$-0.046_{\pm 0.013}$	Riess et al. (2018b)	MW Cepheids
$-0.049_{\pm 0.018}$	Groenewegen (2018)	MW Cepheids
$-0.053_{\pm 0.003}$	Zinn et al. (2019)	Red giants
$-0.054_{\pm 0.006}$	Schönrich et al. (2019)	GDR2 RV
$-0.057_{\pm 0.003}$	Muraveva et al. (2018)	RR Lyrae
$-0.070_{\pm 0.010}$	Ripepi et al. (2019)	LMC Cepheids
$-0.082_{\pm 0.033}$	Stassun & Torres (2018)	Eclipsing binaries

stars of the sample δ Cep and α UMi have no valid parallax value in GDR2, so using their companion parallax allows to include these two precise measurements into the fit. In the following sections, we only use the companion parallaxes. Considering a fixed value of the GDR2 parallax zero point $ZP_{Gaia} = -0.029$ mas, we find the PL and PW relations listed in Table 6.

Table 6. PL and PW relations obtained with the Gaia DR2 parallaxes of Cepheid companions, for a fixed parallax zero-point of −0.029 mas. The equations are of the form $M = a(\log P - 0.77) + b$.

band	a	b	χ^2_r	σ
V	$-2.521_{\pm 0.181}$	$-3.744_{\pm 0.030}$	0.80	0.32
J	$-3.142_{\pm 0.130}$	$-4.807_{\pm 0.018}$	0.64	0.33
H	$-3.304_{\pm 0.423}$	$-5.142_{\pm 0.070}$	2.33	0.35
K_S	$-3.341_{\pm 0.161}$	$-5.125_{\pm 0.031}$	0.85	0.32
W_{VK}	$-3.442_{\pm 0.180}$	$-5.307_{\pm 0.036}$	0.96	0.33
W_H	$-3.481_{\pm 0.535}$	$-5.364_{\pm 0.082}$	3.03	0.36

We can also evaluate the influence of the two additional stars, RS Pup_{echo} and V1334 Cyg, on the quality of the fit. These two stars have a parallax accuracy better than most stars of the sample, so they have an important weight in the fit. Without these two additional stars, the linear fit of the data gives in the K_S band:

$$K_S = -5.130_{\pm 0.038} - 3.227_{\pm 0.329}(\log P - 0.77)$$

with χ^2_r=0.88. When they are taken into account, χ^2_r=0.85 and the PL relation becomes:

$$K_S = -5.125_{\pm 0.031} - 3.341_{\pm 0.161}(\log P - 0.77)$$

The uncertainty on the slope is divided by two when the additional stars are included, and the two equations are consistent within their error bars. We also observe in the upper panel of Fig. 1 that the two corresponding points, represented in red, are in agreement with the other stars of the sample. We therefore include these two stars in our fit of the PL and PW relations.

3.4. Gaia DR2 parallax offset

After the second Gaia data release, many authors found different possible offset values for the parallaxes. Lindegren et al. (2018) used quasars to derive that Gaia parallaxes are underestimated by 0.029 mas. Based on Milky Way Cepheids, Arenou et al. (2018) finds $ZP_{Gaia} = -0.0319$ mas, while Riess et al. (2018b) derive $ZP_{Gaia} = -0.046$ mas. From detached eclipsing binaries and surface brightness-color relations, Graczyk et al. (2019) derived a zero-point shift of −0.031 mas. The recent work of Ripepi et al. (2019) suggested that the GDR2 parallaxes may be underestimated by 0.070 mas. Here we study the influence of the parallax zero-point on the calibration of the CC PL relations. The recent determinations of ZP_{Gaia} are listed in Table 5.

In Table B.2 in Appendix, we list the PL and PW relations obtained for different values of ZP_{Gaia}. In Fig. 3, we represent in blue the intercept as a function of slope of our PL relation in the K_S band, for different values of $\log P$. The different shades of blue represent the different parallax zero-point values: [0; −0.029; −0.046; −0.070] mas, from the lightest to the darkest blue. This diagram shows the influence of ZP_{Gaia} on the calibration of the PL relation slope and intercept. The comparison of our PL relation with other results from the literature will be discussed in Sect. 4.2. Changing the value of ZP_{Gaia} has a relatively small effect on the slope and intercept of the PL relation. For example, most of the recent determinations of ZP_{Gaia} range between 0.029 and 0.070 mas, which corresponds to a change of 0.038 mag for the intercept and 0.051 mag for the slope. This shift is of the order of the error bars of the PL relation. In all bands, rising the value of the offset (that is equivalent to making the zero-point more negative) increases the intercept of PL and PW relations. This results in less luminous CCs, as expected from their increased parallaxes.

In the following sections, we chose to set the GDR2 parallax zero-point to −0.029 mas, as Kervella et al. (2019b) did for their resolved CC companion search.

4. Discussion

4.1. Comparison with the HST/FGS parallax sample

In order to test the quality of the companions GDR2 parallaxes, we compared our calibration of the Leavitt Law in the K_S band with another PL relation based on HST/FGS parallaxes. In this section, we extend the initial sample by including 9 additional stars with HST parallaxes. Those parallaxes are taken from Benedict et al. (2002, 2007) and were measured using the *Fine Guidance Sensor* (FGS) on board the Hubble Space Telescope (HST).

In this sample, only FF Aql is classified as a first overtone by GDR2. We found various results about this CC: while some authors classified it as a fundamental pulsator (Gallenne et al. 2012, from interferometric diameter measurements, van Leeuwen et al. 2007 and Marengo et al. 2010), others claimed it is a first overtone (Feast & Catchpole 1997; Groenewegen 2018; Ripepi et al. 2019) We tried both pulsation modes: considering FF Aql as a

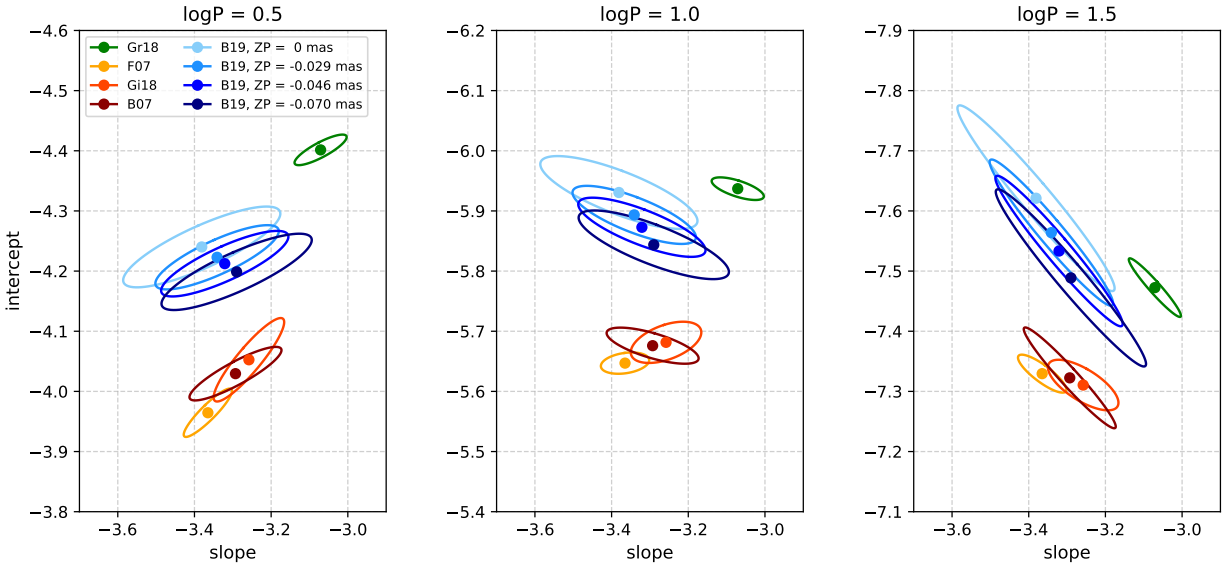

Fig. 3. Comparison of our PL relation obtained in K_S band for different ZP_{Gaia} with other PL relations found in the literature.

References. (Gr18) Groenewegen (2018); (F07) Fouqué et al. (2007); (Gi18) Gieren et al. (2018); (B07) Benedict et al. (2007), (B19) Present work.

fundamental pulsator is in perfect agreement with the fit of the 9 other CCs of Benedict et al. (2007), while assuming it is a first overtone moves the CC away from the PL sequence at more than 3σ. We finally decided to discard FF Aql from the sample for safety.

These nine stars are listed with their data in Table 7. We stress here that only parallaxes were retrieved from Benedict et al. (2002, 2007). The magnitudes are from the Groenewegen (2018) catalog and the color excesses are from the DDO database Fernie et al. (1995), to be consistent with our GDR2 sample.

In order to compare our results with the FGS sample of Benedict et al. (2007), we plot them together on the same PL diagram, in the K_S band (see Fig. 4). The fit of GDR2 data is represented by a blue line and the fit of FGS data is in green. The lower panel shows the residuals in terms of parallax (in mas), which is defined as the difference between the observed parallaxes and the best fit based on the GDR2 parallaxes. The green line in the lower panel represents a parallax excess of 0.25 mas.

We can notice that the PL relation based on FGS parallaxes is shifted towards the bottom of the diagram compared to the relation based on GDR2 parallaxes. This discrepancy may be explained by the presence of an uncorrected Δ_{FGS} zero-point offset of the HST/FGS parallaxes, or a bad choice of the GDR2 parallaxes zero point.

As a first hypothesis, we assume a fixed offset of $ZP_{Gaia} = -0.029$ mas for GDR2 parallaxes and we try to determine a possible ZP for FGS parallaxes. We fix the slope of the FGS sample to the value found for the GDR2 sample. In order to match the FGS points with the GDR2 relation (i.e. to decrease their absolute magnitude), we need to reduce their parallax values. Therefore, we apply a positive zero-point on the FGS parallaxes. The best agreement is found by applying $ZP_{FGS} = 0.23 \pm 0.02$ mas to the HST/FGS parallaxes. Moreover, we notice that the dispersion of FGS points in the PL diagram is substantially improved by this offset correction ($\chi^2 = 0.47$ and $\chi^2 = 0.32$, respectively before and after applying the offset).

Alternatively, we here assume that FGS parallaxes do not need any offset correction and we look for a value of ZP_{Gaia} that would minimize the discrepancy between the two samples. We find that raising the GDR2 offset higher than 0.029 mas increases considerably the dispersion of the GDR2 points ($\chi^2 = 0.85$ and $\chi^2 = 2.16$, respectively with offsets of 0.029 and 0.100 mas). An offset of at least 0.2 mas is needed to match GDR2 points with the FGS fit. Such a high GDR2 zero point seems very unlikely, according to the recent various determinations of ZP_{Gaia} listed in Table 5.

We note that the FGS sample includes the brightest and closest Cepheids, which all have very large parallaxes (1.9 mas $< \varpi <$ 3.66 mas). Contrary to our GDR2 Cepheids, this sample presents an obvious selection on the observed parallaxes, which means that the LKH bias, mentioned in Sect. 3.1, should be corrected, as done by Benedict et al. (2007). As a test, we applied the LKH correction on the FGS sample, with the values from Benedict et al. (2007). This correction yields an offset of 0.19 ± 0.02 mas between the two samples, instead of 0.23 ± 0.02 found without LKH correction. The effect of the LKH correction is not significant, and does not allow us to solve the discrepancy. It is represented as a dashed green line in Fig.4. We also found in Smith (2003) and Francis (2014) that the LKH correction should not be applied in the case of individual stars.

The prototype δ Cep is particularly interesting for this study because it is available in both GDR2 and FGS samples: it hosts a resolved companion, and its parallax has also been measured by the HST/FGS. In addition, it is one of the closest CCs, and has a precise parallax from both techniques: the parallax of its companion from GDR2 is 3.393 ± 0.049 mas and its parallax from HST/FGS is 3.66 ± 0.15 mas. These two points are not in agreement within their error bars. To match the FGS parallax of δ Cep with the GDR2 companion value within 1σ without applying any LKH correction, an offset of -0.27 mas (-7% in relative terms) is necessary on the FGS parallax.

We conclude that FGS parallaxes, whether they take into account the LKH correction or not, are in disagreement with the GDR2 companion parallaxes. This could suggest that FGS parallaxes are likely biased due to an uncorrected zero point offset,

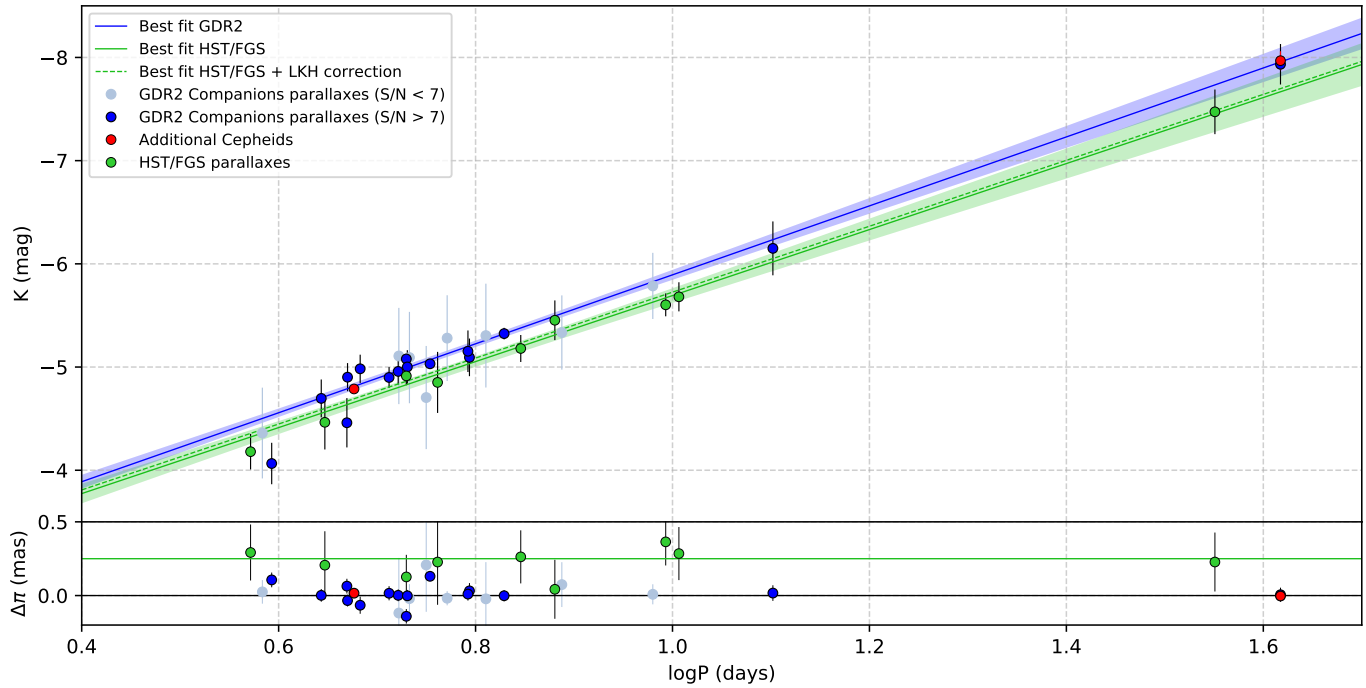

Fig. 4. Period-luminosity relation in the K_S band for the Cepheid companion sample (GDR2 parallaxes) and the Cepheid sample from Benedict et al. (2007) (HST/FGS parallaxes).

Table 7. Data for the Cepheids with HST/FGS parallaxes. The parallaxes and LKH values are from Benedict et al. (2007), $E(B-V)$ from the DDO database (Fernie et al. 1995), V apparent magnitudes from Mel'nik et al. (2015) and J, H, K_S apparent magnitudes from the Groenewegen (2018) catalog, a compilation of apparent magnitudes in different systems from the literature and converted here in the 2MASS system.

Star	Period	ϖ (mas)	$< J >$	$< H >$	$< K_s >$	e_{JHK_s}	ref	$< V >$	E(B-V)	LKH
FF Aql	4.471	$2.81_{\pm 0.18}$	3.854	3.592	3.468	0.010	i	5.37	$0.211_{\pm 0.008}$	-0.03
RT Aur	3.728	$2.40_{\pm 0.19}$	4.284	4.050	3.943	0.008	a	5.45	$0.063_{\pm 0.025}$	-0.05
l Car	35.551	$2.01_{\pm 0.20}$	1.706	1.225	1.073	0.008	b	3.70	$0.163_{\pm 0.017}$	-0.08
δ Cep	5.366	$3.66_{\pm 0.15}$	2.688	2.401	2.299	0.010	c	3.95	$0.080_{\pm 0.019}$	-0.01
ζ Gem	10.151	$2.78_{\pm 0.18}$	2.564	2.217	2.116	0.008	d	3.92	$0.044_{\pm 0.020}$	-0.03
β Dor	9.842	$3.14_{\pm 0.16}$	2.387	2.043	1.943	0.008	b	3.76	$0.080_{\pm 0.015}$	-0.02
W Sgr	7.595	$2.28_{\pm 0.20}$	3.323	2.965	2.801	0.025	e	4.67	$0.116_{\pm 0.011}$	-0.06
X Sgr	7.013	$3.00_{\pm 0.18}$	2.970	2.634	2.511	0.008	d	4.56	$0.201_{\pm 0.021}$	-0.03
Y Sgr	5.773	$2.13_{\pm 0.29}$	4.071	3.713	3.589	0.010	f	5.75	$0.216_{\pm 0.014}$	-0.15
T Vul	4.435	$1.90_{\pm 0.23}$	4.545	4.281	4.179	0.010	c	5.75	$0.098_{\pm 0.018}$	-0.12

References. (a) Monson & Pierce (2011); (b) Laney & Stobie (1992); (c) Barnes et al. (1997); (d) Feast et al. (2008); (e) 2MASS (Skrutskie et al. 2006); (f) Welch et al. (1984)

or it could be explained by a combination of biases on both FGS and Gaia DR2 parallaxes.

4.2. Comparison with other Leavitt law calibrations

We here compare different PL relations from the literature to our results (listed in Table 8). Groenewegen (2018) provides relations in the V, K_S and W_{VK} bands. His work is based on a large sample of CCs whose parallaxes are taken from the GDR2 catalog. This author adopted several different values for GDR2 parallaxes zero point offset. We chose to retrieve his PL relations in the case where he assumes an offset of 0.029 mas, as it is the value that we decided to apply to our sample. Fouqué et al. (2007) derived PL relations in the V, J, H and K_S bands from HST/FGS parallaxes and revised Hipparcos distance measurements. Gieren et al. (2018) used an infrared surface brightness (IRSB) Baade-Wesselink method to determine individual distances to CC sample and build PL relations in the V, J and K bands. His PL relation in the K band is expressed in the UKIRT system. According to Carpenter (2001), the difference between K magnitudes in the UKIRT system and in the 2MASS system is of the order of 0.003 mag. We decide to ignore this correction and to compare directly this PL relation with others PL relations in the 2MASS system. Benedict et al. (2007) derived PL relations in V and K bands from the same HST/FGS parallaxes that we used in the previous section, taking into account the LKH correction. Their K magnitudes are in the CIT system, which, contrary to the UKIRT magnitudes, show a small but significant difference with 2MASS magnitudes. In order to compare this PL relation with our results, we converted their K magnitudes from the CIT to the 2MASS system, using the equation from Carpenter (2001). Finally, Riess et al. (2016) used J, H, V and I magnitudes and spatial scanning parallaxes from the HST-WFC3 instrument to derive a PW relation in the Wesenheit W_H band.

Table 8. Comparison of different Leavitt law calibrations obtained from various authors for Milky Way Cepheids. The value of ρ represents the correlation between the slope and the intercept. All equations are of the form $M = b + a\,(\log P - 1)$ where a and b are respectively the slope and intercept of the Leavitt law.

				Intercept			
Source	ρ	V	J	H	K_S	W_{VK}	W_H
B19	0	$-4.324_{\pm 0.051}$	$-5.530_{\pm 0.035}$	$-5.902_{\pm 0.120}$	$-5.893_{\pm 0.048}$	$-6.099_{\pm 0.055}$	$-6.165_{\pm 0.148}$
Gr18	−0.97	$-4.180_{\pm 0.180}$	-	-	$-5.937_{\pm 0.089}$	$-6.169_{\pm 0.082}$	-
F07	−0.97	$-3.953_{\pm 0.079}$	$-5.258_{\pm 0.071}$	$-5.543_{\pm 0.067}$	$-5.647_{\pm 0.066}$	-	-
Gi18	0	$-3.986_{\pm 0.038}$	$-5.241_{\pm 0.034}$	-	$-5.682_{\pm 0.034}$	-	-
B07	0.7	$-4.050_{\pm 0.020}$	-	-	$-5.676_{\pm 0.030}$	-	-
R16	-	-	-	-	-	-	−5.930
				Slope			
Source	ρ	V	J	H	K_S	W_{VK}	W_H
B19	0	$-2.521_{\pm 0.181}$	$-3.142_{\pm 0.130}$	$-3.304_{\pm 0.423}$	$-3.341_{\pm 0.161}$	$-3.442_{\pm 0.180}$	$-3.481_{\pm 0.535}$
Gr18	−0.97	$-2.305_{\pm 0.136}$	-	-	$-3.071_{\pm 0.068}$	$-3.170_{\pm 0.063}$	-
F07	−0.97	$-2.678_{\pm 0.076}$	$-3.194_{\pm 0.068}$	$-3.328_{\pm 0.064}$	$-3.365_{\pm 0.063}$	-	-
Gi18	0	$-2.615_{\pm 0.100}$	$-3.114_{\pm 0.092}$	-	$-3.258_{\pm 0.092}$	-	-
B07	0.7	$-2.430_{\pm 0.120}$	-	-	$-3.293_{\pm 0.120}$	-	-
R16	-	-	-	-	-	-	−3.260

Notes. (B19) GDR2 parallaxes of companions; (Gr18) Groenewegen (2018), GDR2 parallaxes of Cepheids (ZP_{Gaia} = -0.029 mas); (F07) Fouqué et al. (2007), HST/FGS parallaxes + Hipparcos; (Gi18) Gieren et al. (2018), IRSB method; (B07) Benedict et al. (2007), HST/FGS parallaxes; (R16) Riess et al. (2016).

In Fig. 3 we represent the intercept against the slope of PL relations in the K_S band for different values of $\log P$. In the present work, we find a slope comparable to the values of Fouqué et al. (2007), Benedict et al. (2007), and Gieren et al. (2018). However, the slope found by Groenewegen (2018) is shallower than our value, while our intercept is larger than the one found by Groenewegen (2018). Our intercept is however $\approx$ 0.2 mag smaller than Gieren et al. (2018), Fouqué et al. (2007) and Benedict et al. (2007). This result confirms the difference of 0.2 mag in the PL intercept between the HST/FGS and GDR2 that we found previously. The uncertainties on slopes and intercepts, represented by ellipses, are on the same order as those found by the other authors. This confirms that the PL relations that we found with the GDR2 parallaxes of CC companions are comparable in terms of accuracy to other calibrations found in the literature. The difference between our results and the literature calibrations obtained through the Baade-Wesselink technique can be traced back to HST/FGS parallaxes. As this is the case for Fouqué et al. (2007), the PL calibrations based on distances all rely on the HST/FGS parallaxes for the determination of the projection factor. A discussion of the importance of this parameter can be found, e.g., in Breitfelder et al. (2016). This is the case, e.g., for Gieren et al. (2018), for which the p-factor calibration is from Storm et al. (2011), therefore based on the HST/FGS sample. Our PL relations are represented with other results from the literature in Appendix C.

In order to compare the different PL parameters, zero-point and slope from Table 8, we had to recover for each reference the correlation between the zero-point and the slope. This is very important for a typical CC data set, since the zero-point is usually defined for P=1 day ($\log P = 0$), which is outside the range of the actual Cepheid periods. This results in a very high correlation between the fitted slope and zero-point. In our case, we define $\log P_0$ such as the correlation is null.

Unfortunately, the other published PL calibrations neither use an intercept reference period centered within their CC sample, nor include the correlation coefficients. For Fouqué et al. (2007) and Benedict et al. (2007), the data sets are published so we could compute the correlations. For Gieren et al. (2018), the periods are centered around $< \log P >= 1.18$, so we can assume that the correlation is not significantly different from 0 (assuming that the uncertainties on the magnitudes are all the same). For Groenewegen (2018), we made an educated guess: the data set is very similar to the one from Fouqué et al. (2007), hence we assumed the correlation to be similar (0.97). We should note that for Fouqué et al. (2007), we did not use the published uncertainty on the zero point (i.e., ±0.019 for the K band) since it is not statistically correct. It corresponds to the dispersion of the residuals around the linear fit. However, if one centers the linear fit using the proper $\log P_0$, then the zero-point has indeed this uncertainty, but not at $\log P = 0$.

4.3. Implications for the Hubble constant

Two recent determinations of the Hubble constant H_0 exhibit a tension at the 4.4σ level:

- The empirical estimation by Riess et al. (2019) who obtained $H_0 = 74.03 \pm 1.42\,\mathrm{km\,s^{-1}\,Mpc^{-1}}$ based on LMC Cepheids combined with masers in NGC 4258 and Milky Way parallaxes,
- The value $H_0 = 67.4 \pm 0.5\,\mathrm{km\,s^{-1}\,Mpc^{-1}}$ derived from the Planck CMB data by Planck Collaboration et al. (2018), assuming a ΛCDM cosmology.

Riess et al. (2019) (hereafter R19) established a PL relation in the Wesenheit W_H index for LMC Cepheids, assuming the 1.2 % geometric distance from Pietrzyński et al. (2019) based on LMC eclipsing binaries. They find :

$$m_{W_H} = 15.898 - 3.26\ \log P \quad (1)$$

This PL relation includes the CNRL correction on apparent magnitudes, a systematic effect that appears while observing faint and bright sources with the WFC3 instrument (see Riess et al. 2019), and corrections for the LMC geometry.

They combined this PL calibration with two other anchors, masers in NGC 4258 and parallaxes of MW Cepheids from the HST, and they derived $H_0 = 74.03 \pm 1.42\,\mathrm{km\,s^{-1}\,Mpc^{-1}}$. The

H_0 value based on the LMC Cepheid anchor only is 74.22 ± 1.42 km s^{-1} Mpc^{-1}.

Following the method given in Section 4 of Riess et al. (2018a), we can translate our results into a new value of the Hubble constant $H_{0,\mathrm{Gaia}}$ based on our PL calibration with the GDR2 parallaxes of Milky Way CC companions. Here we rescale the R19 value from LMC Cepheid anchor only, through the relation $H_{0,\mathrm{Gaia}} = \alpha\, H_{0,\mathrm{R19}}$ where $\alpha = \varpi_{\mathrm{Gaia}}/\varpi_{\mathrm{R19}}$. In terms of magnitudes, this relation gives :

$$H_{0,\mathrm{Gaia}} = H_{0,\mathrm{R19}}\, 10^{0.2\,(W_{H,\mathrm{Gaia}} - m_{W_H} + \mu_{\mathrm{LMC}})} \quad (2)$$

where $W_{H,\mathrm{Gaia}}$ is obtained from the GDR2 companion parallaxes, m_{W_H} is given by Eq. 1, and μ_{LMC} = 18.477 mag is the LMC distance modulus from Pietrzyński et al. (2019). We correct for the metallicity term by applying an additional term $\gamma[Fe/H]$, with [Fe/H]$_{\mathrm{LMC}}$=-0.33 dex and γ = -0.17 mag dex^{-1}, as given in R19. We make the assumption that the MW metallicity correction is null, given that [Fe/H] = +0.00 ± 0.05 dex (Romaniello et al. 2008). For each Cepheid of the GDR2 sample and for the two additional stars, we compute an individual H_0, and we derive $H_{0,\mathrm{Gaia}}$ as the weighted mean of these values.

The results, which depend on the value of GDR2 offset, are listed in Table 9 and represented in Fig. 6. The uncertainties take into account the error on $H_{0\,\mathrm{R19}}$, on μ_{LMC} and the dispersion of both PL relations. We find that the $H_{0,\mathrm{Gaia}}$ value follows the linear relation: $H_{0,\mathrm{Gaia}} = 66.93 - 51.22\,\mathrm{ZP}_{\mathrm{Gaia}}$ where $\mathrm{ZP}_{\mathrm{Gaia}}$ is in mas.

Table 9. Rescaling of H_0 based on the GDR2 parallaxes of companions, for different values of $\mathrm{ZP}_{\mathrm{Gaia}}$.

$\mathrm{ZP}_{\mathrm{Gaia}}$ (mas)	$H_{0,\mathrm{Gaia}}$ (km s^{-1} Mpc^{-1})
0	66.93 ± 2.07
-0.029	68.43 ± 2.08
-0.046	69.30 ± 2.08
-0.070	70.53 ± 2.08
-0.090	71.54 ± 2.09

We can also adopt a similar approach by fixing the slope to the value given by R19 in Eq. 1, and by comparing the zero points of the two PW relations. Applying this method leads to a smaller value of 67 ± 2 km s^{-1} Mpc^{-1}, for a zero point offset between 0.029 mas and 0.046 mas. This is consistent at 1σ with the results obtained with the first approach.

In Fig. 5, we represent the distance modulus of the stars of our sample μ_{Gaia} computed from GDR2 companions parallaxes, against the distance modulus computed with the PW relation from R19. It appears that, as a global trend, GDR2 exhibit smaller distance modulus compared to R19. The distances of all of the stars with S/N >10 are larger with R19 than with GDR2, resulting in a lower value of $H_{0,\mathrm{Gaia}}$.

As we saw in Sect. 3.4, the value of $\mathrm{ZP}_{\mathrm{Gaia}}$ has an impact on the PL relation : chosing different values of $\mathrm{ZP}_{\mathrm{Gaia}}$ will lead to various results for H_0. On Fig. 6 are represented in blue our values of $H_{0,\mathrm{Gaia}}$ as a function of $\mathrm{ZP}_{\mathrm{Gaia}}$. The value of $H_{0,\mathrm{Gaia}}$ increases linearly with Gaia parallaxes offset. Our results are in agreement with Planck Collaboration et al. (2018) within the error bars for $\mathrm{ZP}_{\mathrm{Gaia}}$ between 0 mas and 0.060 mas, and consistent with the value found by R19 anchored to Cepheids for a GDR2 offset larger than 0.065 mas.

Assuming a GDR2 parallax offset between 0.029 and 0.046 mas, we find $H_{0,\mathrm{Gaia}} \sim 69 \pm 2$ km s^{-1} Mpc^{-1}, in agreement with Planck Collaboration et al. (2018), and compatible with the recent determination by Freedman et al. (2019) based on the Tip

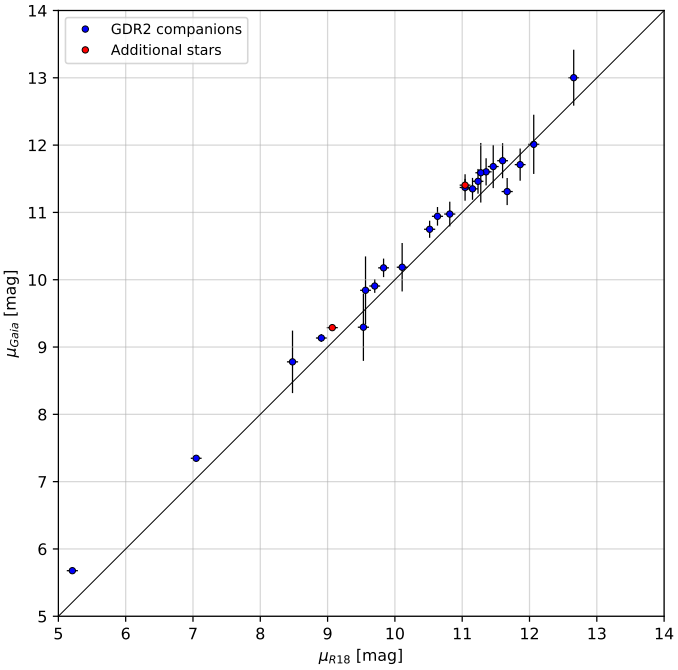

Fig. 5. Distance ladder: distance modulus of the stars of our sample according to R19 and according to Gaia parallaxes of companions.

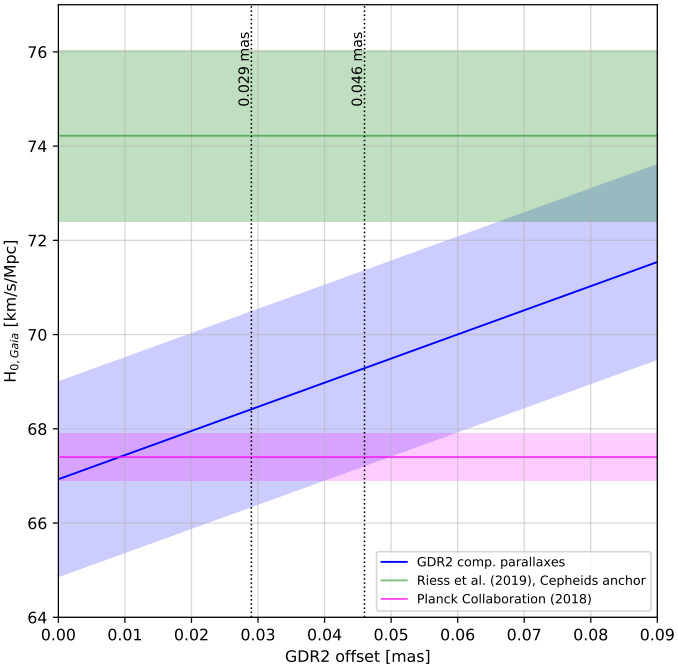

Fig. 6. Rescaling of R19 Hubble constant from Cepheids anchor only, against the GDR2 parallaxes offset.

on the Red Giant Branch. The next Gaia data releases are expected to improve the precision on parallaxes and hopefully fix the offset, allowing us to reduce the uncertainties on the Hubble constant.

5. Conclusion

We presented a new calibration of the Leavitt law of Milky Way CCs based on the GDR2 parallax measurements of resolved Cepheid companions. Thanks to the absence of large amplitude

photometric and color variability of these companions, this original approach allows us to bypass the uncertain reliability of the GDR2 parallaxes of the CCs themselves. A comparison of our calibration with previous works based on HST/FGS parallaxes of nearby CCs indicates that a significant parallax zero-point offset may be present in these measurements.

For the most commonly admitted values of the GDR2 parallax offset (between 0.029 mas and 0.050 mas), the translation of our PL relation calibration in terms of scaling of the Hubble constant results in a value of 69 ± 2 km s^{-1} Mpc^{-1}, statistically compatible with the Planck Collaboration et al. (2018) estimate.

The inclusion of the variability of the CCs in the astrometric processing of the third Gaia data release will provide high precision trigonometric parallaxes of a large sample of MW CCs (Clementini et al. 2018), allowing to study in details the influence of metallicity on PL relations. This will result in a very accurate calibration of the Leavitt law in the Milky Way, based purely on trigonometric parallaxes, and consequently in a more direct and reliable estimate of the Hubble constant.

Acknowledgements. The research leading to these results has received funding from the European Research Council (ERC) under the European Union's Horizon 2020 research and innovation programme under grant agreement No 695099 (project CepBin). This work has made use of data from the European Space Agency (ESA) mission Gaia (http://www.cosmos.esa.int/gaia), processed by the Gaia Data Processing and Analysis Consortium (DPAC, http://www.cosmos.esa.int/web/gaia/dpac/consortium). Funding for the DPAC has been provided by national institutions, in particular the institutions participating in the Gaia Multilateral Agreement. The authors acknowledge the support of the French Agence Nationale de la Recherche (ANR), under grant ANR-15-CE31-0012-01 (project UnlockCepheids). W.G. and G.P. gratefully acknowledge financial support for this work from the BASAL Centro de Astrofisica y Tecnologias Afines (CATA) AFB-170002. W.G. acknowledges financial support from the Millenium Institute of Astrophysics (MAS) of the Iniciativa Cientifica Milenio del Ministerio de Economia, Fomento y Turismo de Chile, project IC120009. We acknowledge support from the IdP II 2015 0002 64 grant of the Polish Ministry of Science and Higher Education. This research made use of Astropy7, a community-developed core Python package for Astronomy (Astropy Collaboration et al. 2013). We used the SIMBAD and VIZIER databases and catalogue access tool at the CDS, Strasbourg (France), and NASA's Astrophysics Data System Bibliographic Services. This publication makes use of data products from the Two Micron All Sky Survey, which is a joint project of the University of Massachusetts and the Infrared Processing and Analysis Center/California Institute of Technology, funded by the National Aeronautics and Space Administration and the National Science Foundation.

References

Arenou, F. & Luri, X. 1999, in Astronomical Society of the Pacific Conference Series, Vol. 167, Harmonizing Cosmic Distance Scales in a Post-HIPPARCOS Era, ed. D. Egret & A. Heck, 13–32
Arenou, F., Luri, X., Babusiaux, C., et al. 2018, A&A, 616, A17
Barnes, III, T. G., Fernley, J. A., Frueh, M. L., et al. 1997, PASP, 109, 645
Benedict, G. F., McArthur, B. E., Feast, M. W., et al. 2007, AJ, 133, 1810
Benedict, G. F., McArthur, B. E., Fredrick, L. W., et al. 2002, AJ, 124, 1695
Berdnikov, L. N., Dambis, A. K., & Vozyakova, O. V. 2000, A&AS, 143, 211
Bono, G., Gieren, W. P., Marconi, M., & Fouqué, P. 2001, ApJ, 552, L141
Breitfelder, J., Mérand, A., Kervella, P., et al. 2016, A&A, 587, A117
Carpenter, J. M. 2001, AJ, 121, 2851
Casertano, S., Riess, A. G., Anderson, J., et al. 2016, ApJ, 825, 11
Clementini, G., Garofalo, A., Muraveva, T., & Ripepi, V. 2018, in Astronomical Society of the Pacific Conference Series, Vol. 514, Stellar Populations and the Distance Scale, ed. J. Jensen, 89
Clementini, G., Ripepi, V., Molinaro, R., et al. 2019, A&A, 622, A60
Di Benedetto, G. P. 2002, AJ, 124, 1213
Drimmel, R., Bucciarelli, B., & Inno, L. 2019, Research Notes of the American Astronomical Society, 3, 79
Droege, T. F., Richmond, M. W., Sallman, M. P., & Creager, R. P. 2006, PASP, 118, 1666
Epchtein, N., Deul, E., Derriere, S., et al. 1999, A&A, 349, 236
ESA, ed. 1997, ESA Special Publication, Vol. 1200, The HIPPARCOS and TYCHO catalogues. Astrometric and photometric star catalogues derived from the ESA HIPPARCOS Space Astrometry Mission
Evans, N. R., Arellano Ferro, A., & Udalska, J. 1992, AJ, 103, 1638
Feast, M. W. & Catchpole, R. M. 1997, MNRAS, 286, L1
Feast, M. W., Laney, C. D., Kinman, T. D., van Leeuwen, F., & Whitelock, P. A. 2008, MNRAS, 386, 2115
Fernie, J. D., Evans, N. R., Beattie, B., & Seager, S. 1995, Information Bulletin on Variable Stars, 4148
Fitzpatrick, E. L. 1999, PASP, 111, 63
Fouqué, P., Arriagada, P., Storm, J., et al. 2007, A&A, 476, 73
Francis, C. 2014, MNRAS, 444, L6
Freedman, W. L., Madore, B. F., Gibson, B. K., et al. 2001, ApJ, 553, 47
Freedman, W. L., Madore, B. F., Hatt, D., et al. 2019, arXiv e-prints, arXiv:1907.05922
Gaia Collaboration, Brown, A. G. A., Vallenari, A., et al. 2018, A&A, 616, A1
Gaia Collaboration, Clementini, G., Eyer, L., et al. 2017, A&A, 605, A79
Gaia Collaboration, Eyer, L., Rimoldini, L., et al. 2019, A&A, 623, A110
Gallenne, A., Kervella, P., Evans, N. R., et al. 2018, ApJ, 867, 121
Gallenne, A., Kervella, P., Mérand, A., et al. 2012, A&A, 541, A87
Gallenne, A., Kervella, P., Mérand, A., et al. 2017, A&A, 608, A18
Gallenne, A., Mérand, A., Kervella, P., et al. 2014, A&A, 561, L3
Genovali, K., Lemasle, B., Bono, G., et al. 2014, A&A, 566, A37
Gieren, W., Storm, J., Konorski, P., et al. 2018, A&A, 620, A99
Graczyk, D., Pietrzyński, G., Gieren, W., et al. 2019, ApJ, 872, 85
Groenewegen, M. A. T. 2018, A&A, 619, A8
Groenewegen, M. A. T. & Oudmaijer, R. D. 2000, A&A, 356, 849
Hall, O. J., Davies, G. R., Elsworth, Y. P., et al. 2019, MNRAS, 1036
Hanson, R. B. 1979, MNRAS, 186, 875
Kervella, P., Arenou, F., Mignard, F., & Thévenin, F. 2019a, A&A, 623, A72
Kervella, P., Bond, H. E., Cracraft, M., et al. 2014, A&A, 572, A7
Kervella, P., Gallenne, A., Evans, N. R., et al. 2019b, A&A, 623, A117
Kervella, P., Trahin, B., Bond, H. E., et al. 2017, A&A, 600, A127
Koen, C. & Laney, D. 1998, MNRAS, 301, 582
Koen, C., Marang, F., Kilkenny, D., & Jacobs, C. 2007, MNRAS, 380, 1433
Kovtyukh, V. V., Luck, R. E., Chekhonadskikh, F. A., & Belik, S. I. 2012, MNRAS, 426, 398
Kovtyukh, V. V., Soubiran, C., Luck, R. E., et al. 2008, MNRAS, 389, 1336
Laney, C. D. & Caldwell, J. A. R. 2007, MNRAS, 377, 147
Laney, C. D. & Stobie, R. S. 1992, A&AS, 93, 93
Leavitt, H. S. 1908, Annals of Harvard College Observatory, 60, 87
Leavitt, H. S. & Pickering, E. C. 1912, Harvard College Observatory Circular, 173, 1
Lemos, P., Lee, E., Efstathiou, G., & Gratton, S. 2019, MNRAS, 483, 4803
Lindegren, L. 2018a, Gaia DR2 astrometry
Lindegren, L. 2018b, Re-normalising the astrometric chi-square in Gaia DR2, Tech. Rep. GAIA-C3-TN-LU-LL-124, Lund Observatory
Lindegren, L. 2019, arXiv e-prints, arXiv:1906.09827
Lindegren, L., Hernández, J., Bombrun, A., et al. 2018, A&A, 616, A2
Luck, R. E. 2018, AJ, 156, 171
Lutz, T. E. & Kelker, D. H. 1973, PASP, 85, 573
Marengo, M., Evans, N. R., Barmby, P., et al. 2010, ApJ, 709, 120
Mel'nik, A. M., Rautiainen, P., Berdnikov, L. N., Dambis, A. K., & Rastorguev, A. S. 2015, Astronomische Nachrichten, 336, 70
Mérand, A., Kervella, P., Breitfelder, J., et al. 2015, A&A, 584, A80
Monson, A. J. & Pierce, M. J. 2011, ApJS, 193, 12
Mowlavi, N., Lecoeur-Taïbi, I., Lebzelter, T., et al. 2018, A&A, 618, A58
Muraveva, T., Delgado, H. E., Clementini, G., Sarro, L. M., & Garofalo, A. 2018, MNRAS, 481, 1195
Ngeow, C.-C. & Kanbur, S. M. 2006, MNRAS, 369, 723
Oudmaijer, R. D., Groenewegen, M. A. T., & Schrijver, H. 1998, MNRAS, 294, L41
Pietrzyński, G., Graczyk, D., Gallenne, A., et al. 2019, Nature, 567, 200
Planck Collaboration, Aghanim, N., Akrami, Y., et al. 2018, arXiv e-prints [arXiv:1807.06209]
Pont, F. 1999, in Astronomical Society of the Pacific Conference Series, Vol. 167, Harmonizing Cosmic Distance Scales in a Post-HIPPARCOS Era, ed. D. Egret & A. Heck, 113–128
Riess, A. G., Casertano, S., Anderson, J., MacKenty, J., & Filippenko, A. V. 2014, ApJ, 785, 161
Riess, A. G., Casertano, S., Yuan, W., et al. 2018a, ApJ, 855, 136
Riess, A. G., Casertano, S., Yuan, W., et al. 2018b, ApJ, 861, 126
Riess, A. G., Casertano, S., Yuan, W., Macri, L. M., & Scolnic, D. 2019, ApJ, 876, 85
Riess, A. G., Macri, L. M., Hoffmann, S. L., et al. 2016, ApJ, 826, 56
Ripepi, V., Molinaro, R., Musella, I., et al. 2019, A&A, 625, A14
Ripepi, V., Moretti, M. I., Marconi, M., et al. 2012, MNRAS, 424, 1807
Romaniello, M., Primas, F., Mottini, M., et al. 2008, A&A, 488, 731
Sahlholdt, C. L. & Silva Aguirre, V. 2018, MNRAS, 481, L125
Sandage, A., Tammann, G. A., & Reindl, B. 2004, A&A, 424, 43
Sandage, A., Tammann, G. A., Saha, A., et al. 2006, ApJ, 653, 843
Schechter, P. L., Avruch, I. M., Caldwell, J. A. R., & Keane, M. J. 1992, AJ, 104, 1930

Schönrich, R., McMillan, P., & Eyer, L. 2019, MNRAS, 487, 3568
Skrutskie, M. F., Cutri, R. M., Stiening, R., et al. 2006, AJ, 131, 1163
Smith, H. 2003, MNRAS, 338, 891
Spreckley, S. & Stevens, I. R. 2007, in Astronomical Society of the Pacific Conference Series, Vol. 366, Transiting Extrapolar Planets Workshop, ed. C. Afonso, D. Weldrake, & T. Henning, 39
Stassun, K. G. & Torres, G. 2018, ApJ, 862, 61
Storm, J., Gieren, W., Fouqué, P., et al. 2011, A&A, 534, A94
Usenko, I. A., Kniazev, A. Y., Berdnikov, L. N., & Kravtsov, V. V. 2014, Astronomy Letters, 40, 800
van Leeuwen, F., Feast, M. W., Whitelock, P. A., & Laney, C. D. 2007, MNRAS, 379, 723
Welch, D. L., Wieland, F., McAlary, C. W., et al. 1984, ApJS, 54, 547
Zabolotskikh, M. V., Rastorguev, A. S., & Egorov, I. E. 2004, in Astronomical Society of the Pacific Conference Series, Vol. 316, Order and Chaos in Stellar and Planetary Systems, ed. G. G. Byrd, K. V. Kholshevnikov, A. A. Myllri, I. I. Nikiforov, & V. V. Orlov, 209
Zinn, J. C., Pinsonneault, M. H., Huber, D., & Stello, D. 2019, ApJ, 878, 136

Appendix A: Results of the bootstrap technique

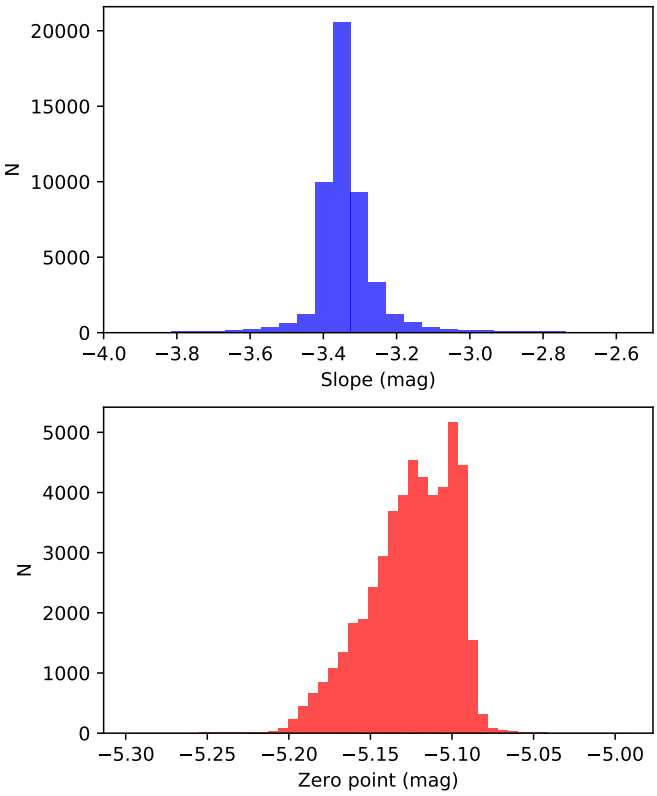

Fig. A.1. Results of the bootstrap technique applied on the fit of the Leavitt law in the K_S band based on companions GDR2 parallaxes.

Appendix B: Influence of the parallaxes and of the zero point on the calibration of the Leavitt Law

Table B.1. PL and PW relations obtained with Gaia DR2 parallaxes of CCS companions and with Gaia DR2 parallaxes of CCs themselves. The GDR2 parallaxes offset is assumed to be 0.029 mas. The equations are of the form $M = a(\log P - 0.77) + b$.

band	a	b	χ^2_r	σ
Parallaxes of Companions				
V	$-2.521_{\pm 0.181}$	$-3.744_{\pm 0.030}$	2.96	0.32
J	$-3.142_{\pm 0.130}$	$-4.807_{\pm 0.018}$	0.81	0.33
H	$-3.304_{\pm 0.423}$	$-5.142_{\pm 0.070}$	2.35	0.35
K_S	$-3.341_{\pm 0.161}$	$-5.125_{\pm 0.031}$	0.85	0.32
W_{VK}	$-3.442_{\pm 0.180}$	$-5.307_{\pm 0.036}$	1.01	0.33
W_H	$-3.481_{\pm 0.535}$	$-5.364_{\pm 0.082}$	2.97	0.36
Parallaxes of Cepheids				
V	$-2.308_{\pm 0.241}$	$-3.779_{\pm 0.049}$	7.63	0.31
J	$-2.939_{\pm 0.212}$	$-4.849_{\pm 0.055}$	3.29	0.34
H	$-3.039_{\pm 0.183}$	$-5.104_{\pm 0.044}$	2.42	0.33
K_S	$-3.142_{\pm 0.214}$	$-5.164_{\pm 0.055}$	2.31	0.34
W_{VK}	$-3.243_{\pm 0.217}$	$-5.345_{\pm 0.055}$	2.04	0.34
W_H	$-3.200_{\pm 0.198}$	$-5.311_{\pm 0.045}$	1.84	0.33

Table B.2. PL and PW relations obtained with Gaia DR2 parallaxes of Cepheid companions, for different parallax zero-points. The equations are of the form $M = a(\log P - 0.77) + b$.

band	a	b	χ^2_r	σ
ZP_{Gaia} = 0 mas				
V	$-2.546_{\pm 0.171}$	$-3.775_{\pm 0.022}$	2.68	0.32
J	$-3.179_{\pm 0.161}$	$-4.836_{\pm 0.024}$	0.83	0.35
H	$-3.351_{\pm 0.439}$	$-5.169_{\pm 0.063}$	1.96	0.35
K_S	$-3.381_{\pm 0.205}$	$-5.153_{\pm 0.038}$	1.01	0.35
W_{VK}	$-3.481_{\pm 0.220}$	$-5.335_{\pm 0.042}$	1.19	0.35
W_H	$-3.527_{\pm 0.559}$	$-5.392_{\pm 0.073}$	2.52	0.36
ZP_{Gaia} = -0.029 mas				
V	$-2.521_{\pm 0.181}$	$-3.744_{\pm 0.030}$	0.80	0.32
J	$-3.142_{\pm 0.130}$	$-4.807_{\pm 0.018}$	0.64	0.33
H	$-3.304_{\pm 0.423}$	$-5.142_{\pm 0.070}$	2.33	0.35
K_S	$-3.341_{\pm 0.161}$	$-5.125_{\pm 0.031}$	0.85	0.32
W_{VK}	$-3.442_{\pm 0.180}$	$-5.307_{\pm 0.036}$	0.96	0.33
W_H	$-3.481_{\pm 0.535}$	$-5.364_{\pm 0.082}$	3.03	0.36
ZP_{Gaia} = -0.046 mas				
V	$-2.500_{\pm 0.218}$	$-3.725_{\pm 0.038}$	3.28	0.33
J	$-3.123_{\pm 0.138}$	$-4.791_{\pm 0.022}$	0.97	0.33
H	$-3.285_{\pm 0.427}$	$-5.126_{\pm 0.076}$	2.78	0.36
K_S	$-3.321_{\pm 0.166}$	$-5.109_{\pm 0.031}$	0.95	0.32
W_{VK}	$-3.422_{\pm 0.176}$	$-5.290_{\pm 0.036}$	1.09	0.32
W_H	$-3.460_{\pm 0.543}$	$-5.349_{\pm 0.087}$	3.42	0.37
ZP_{Gaia} = -0.070 mas				
V	$-2.480_{\pm 0.278}$	$-3.700_{\pm 0.050}$	3.89	0.35
J	$-3.094_{\pm 0.193}$	$-4.768_{\pm 0.030}$	1.43	0.34
H	$-3.256_{\pm 0.457}$	$-5.103_{\pm 0.085}$	3.61	0.38
K_S	$-3.290_{\pm 0.196}$	$-5.087_{\pm 0.035}$	1.32	0.33
W_{VK}	$-3.393_{\pm 0.204}$	$-5.266_{\pm 0.039}$	1.43	0.33
W_H	$-3.429_{\pm 0.554}$	$-5.328_{\pm 0.095}$	4.29	0.39

Appendix C: Leavitt law with GDR2 companions parallaxes

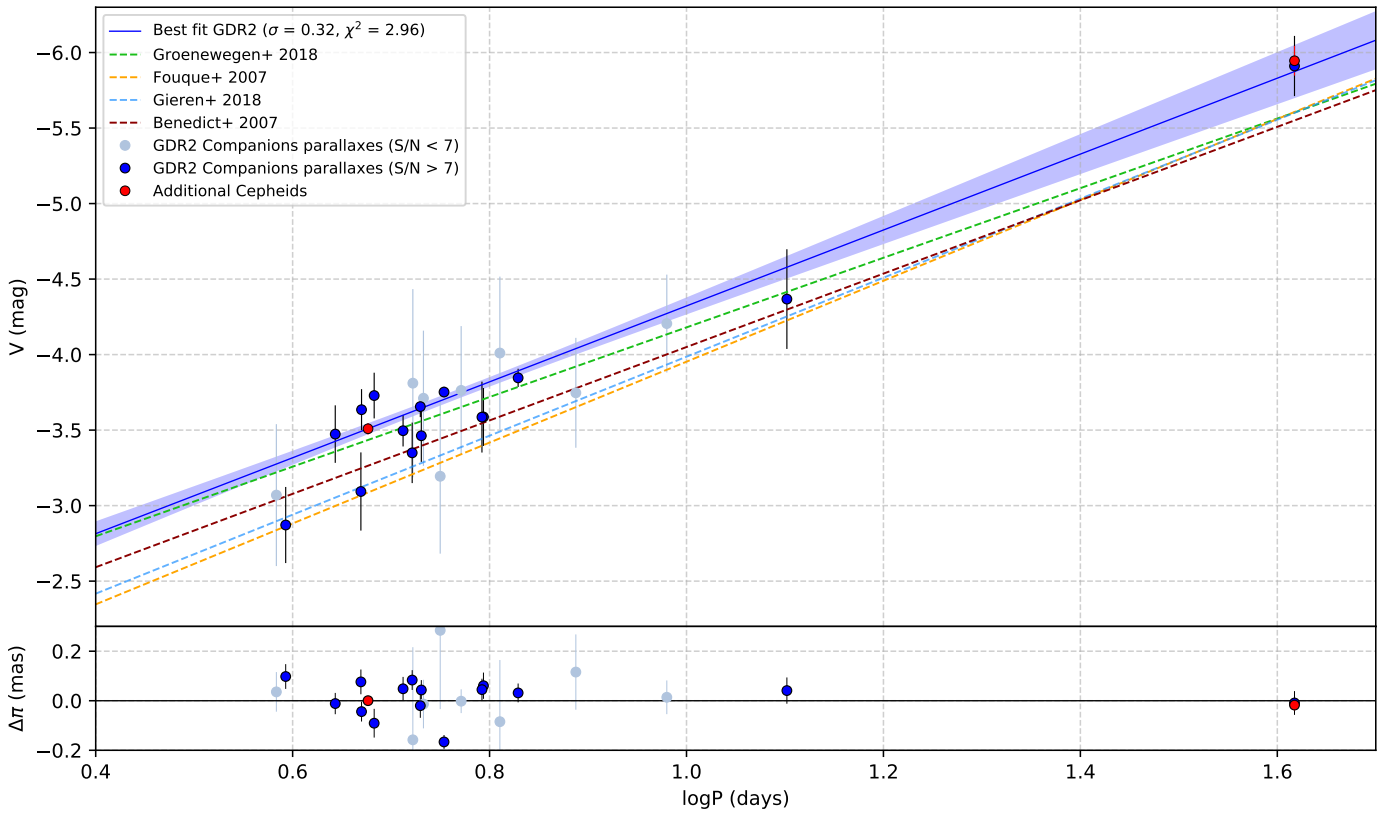

Fig. C.1. PL diagram in the *V* band for GDR2 companions parallaxes.

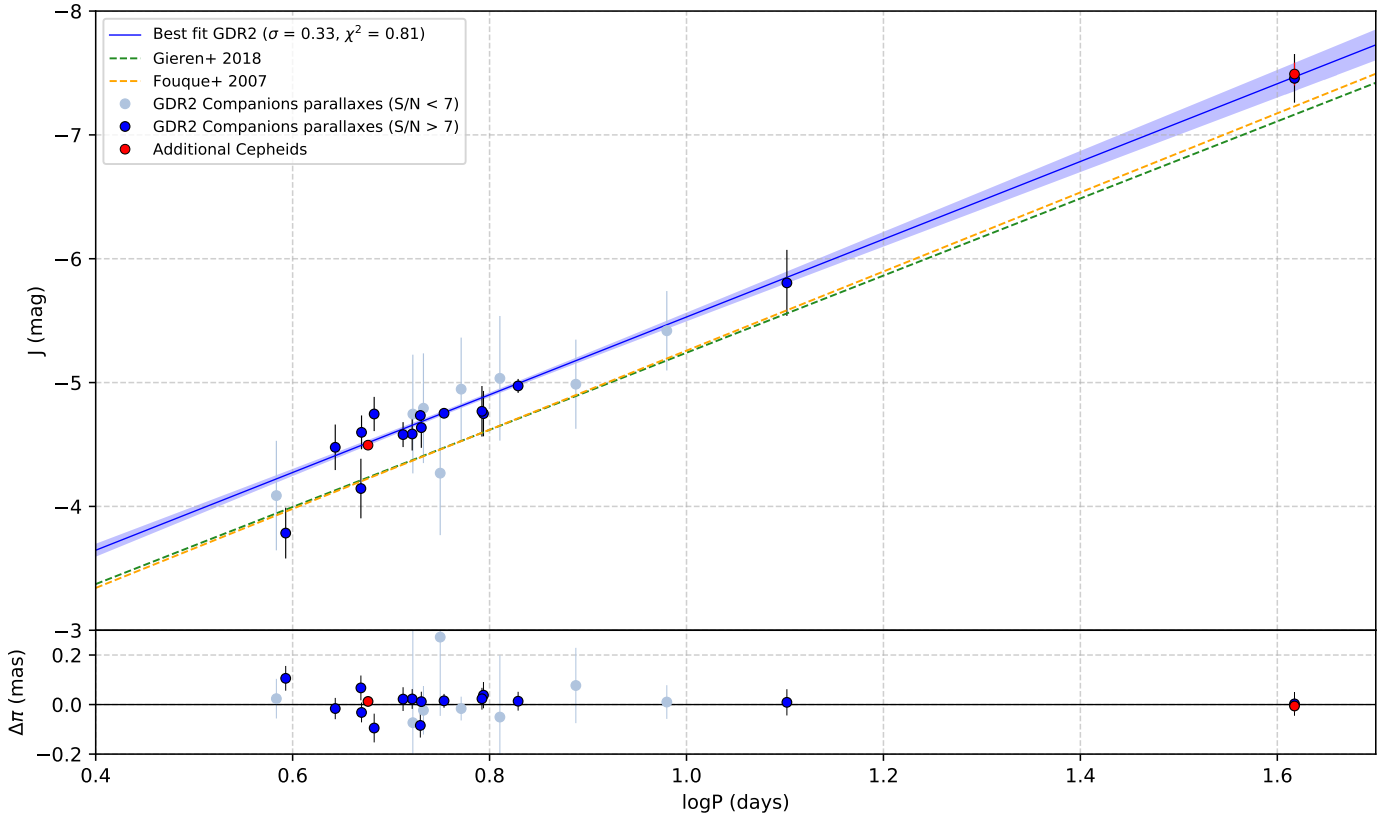

Fig. C.2. PL diagram in the *J* band for GDR2 companions parallaxes.

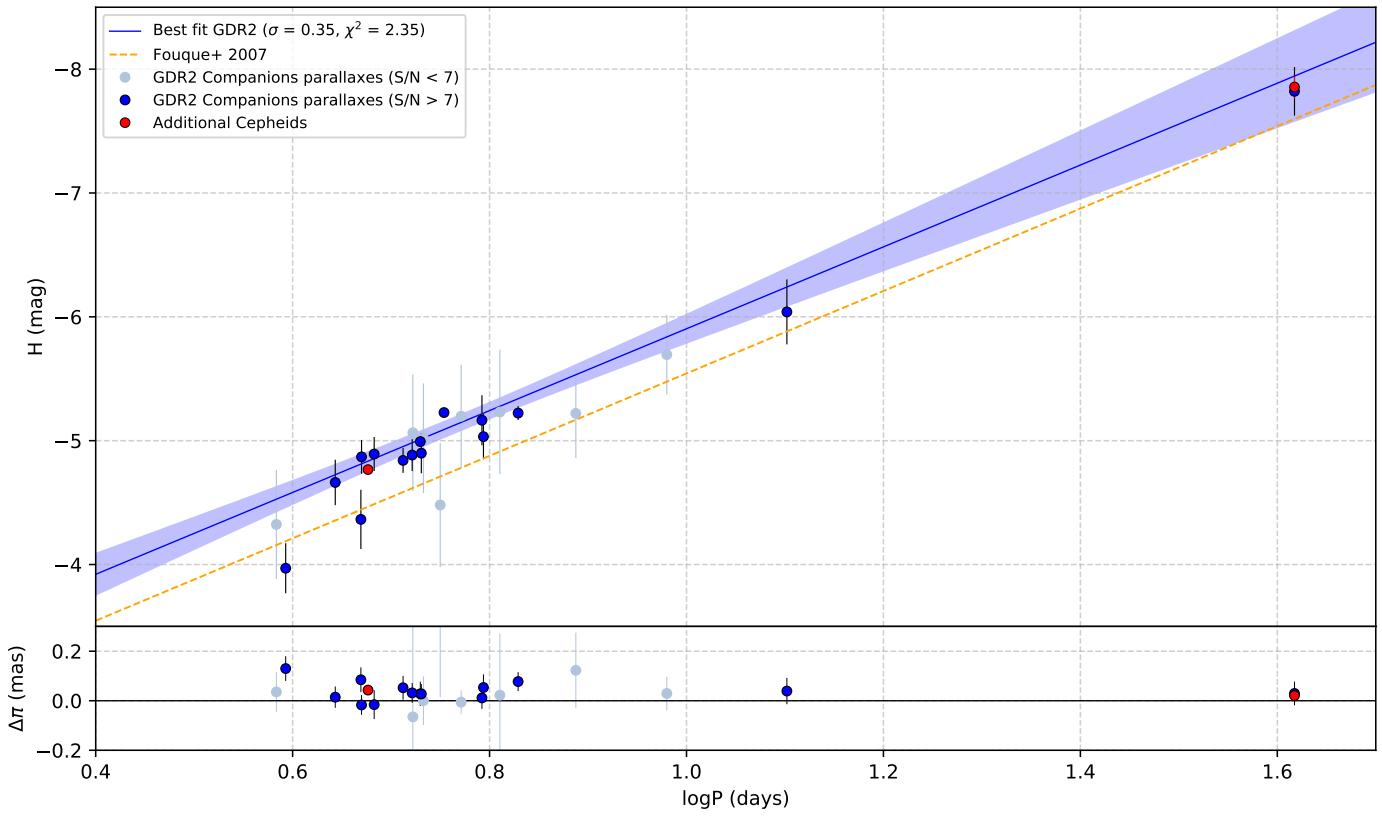

Fig. C.3. PL diagram in the H band for GDR2 companions parallaxes.

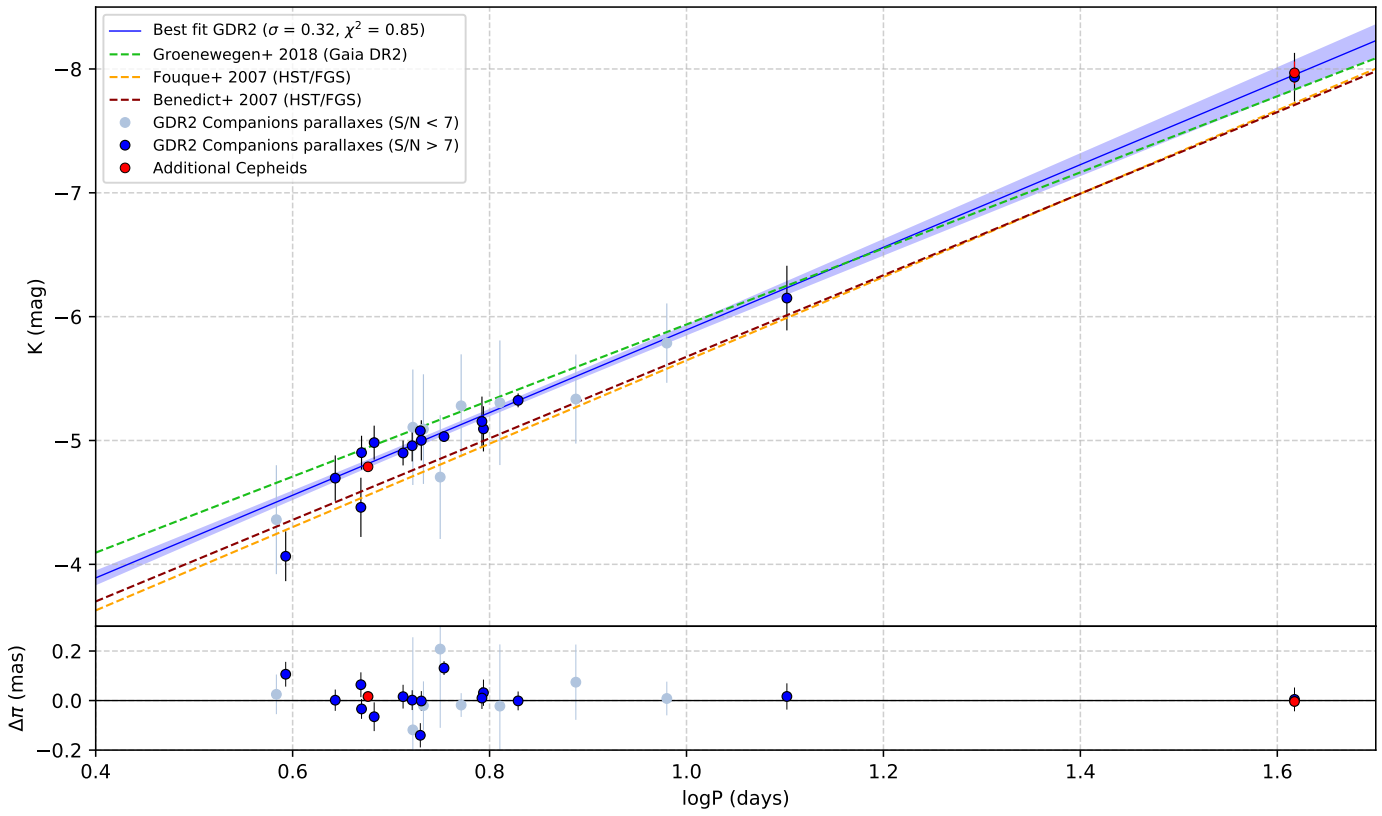

Fig. C.4. PL diagram in the K_S band for GDR2 companions parallaxes.

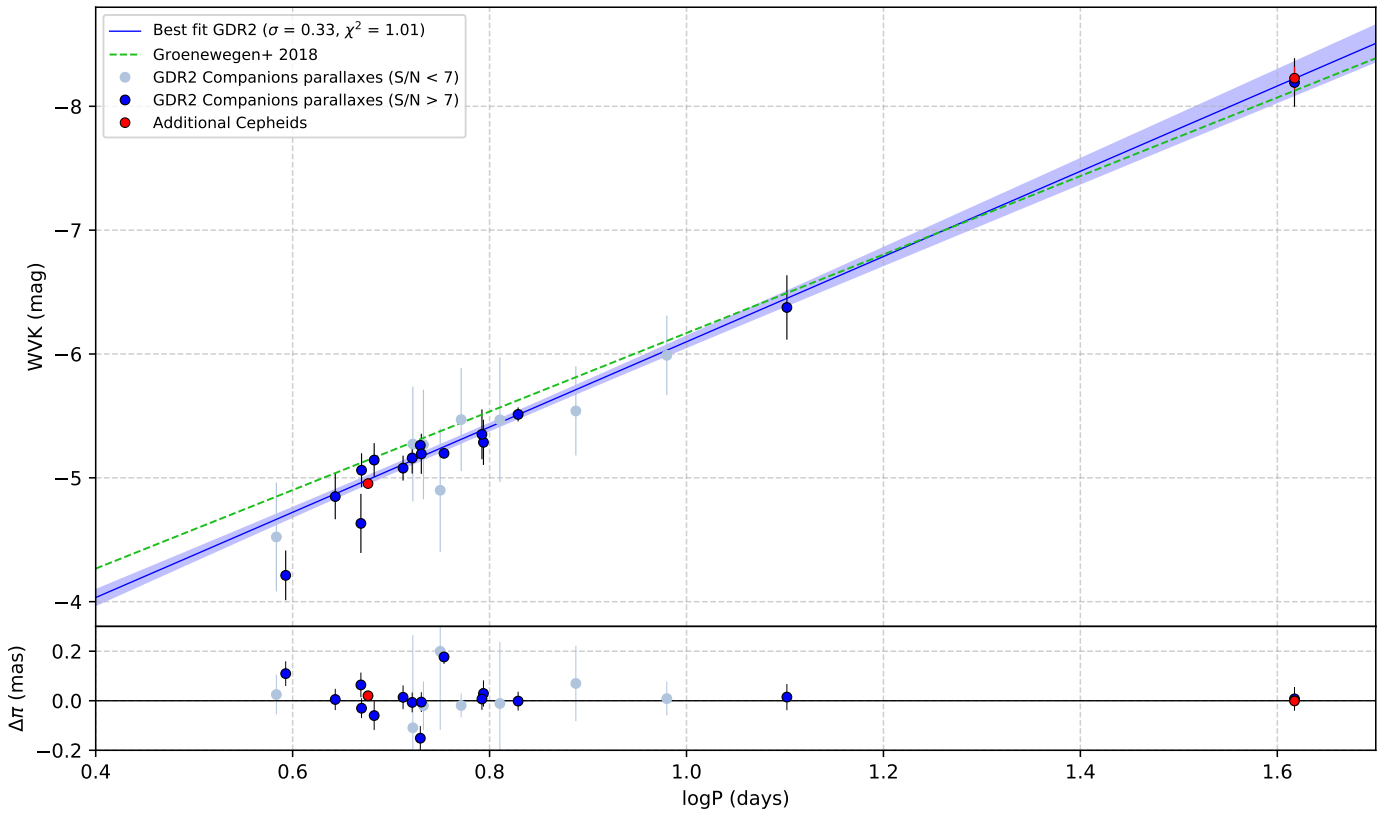

Fig. C.5. PW diagram in the W_{VK} band for GDR2 companions parallaxes.

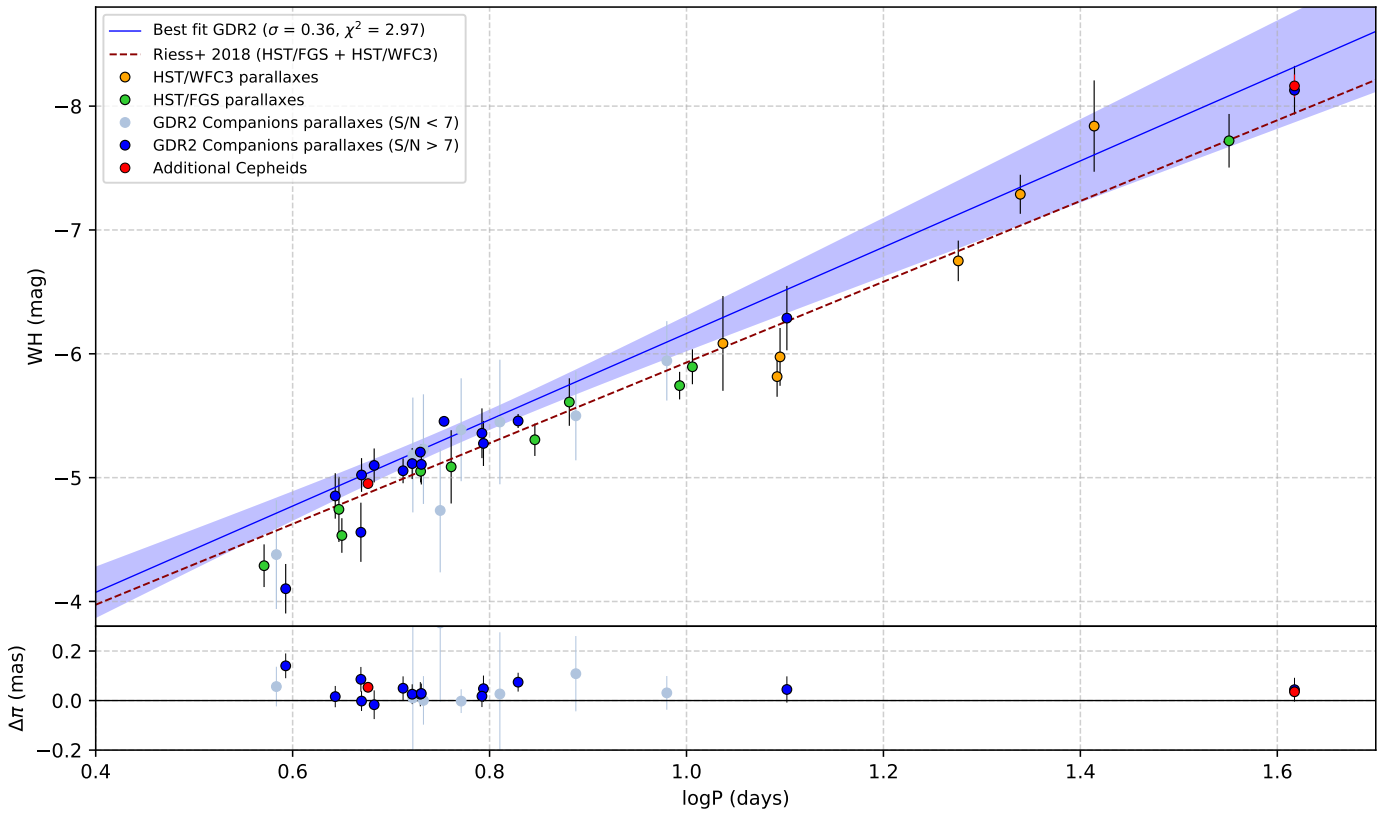

Fig. C.6. PW diagram in the W_H band for GDR2 companions parallaxes. The PW relation found by R18 (dark red dashed line) was calibrated using the parallaxes from HST/FGS (green points) and by spatial scanning with the HST/WFC3 (orange points).